

Efficient fully precessing gravitational waveforms for binaries with neutron stars

Michael LaHaye 

Department of Physics, University of Guelph, Guelph, Ontario, N1G 2W1, Canada

Huan Yang 

*Perimeter Institute for Theoretical Physics, Ontario, N2L 2Y5, Canada
and Department of Physics, University of Guelph, Guelph, Ontario, N1G 2W1, Canada*

Béatrice Bonga 

*Institute for Mathematics, Astrophysics and Particle Physics, Radboud University,
6525 AJ Nijmegen, The Netherlands*

Zhenwei Lyu 

*Kavli Institute for Astronomy and Astrophysics, Peking University, Beijing 100871, China
and Department of Physics, University of Guelph, Guelph, Ontario, N1G 2W1, Canada*



(Received 20 December 2022; accepted 10 July 2023; published 21 August 2023)

We construct an efficient frequency domain waveform for generic circular compact object binaries that include neutron stars. The orbital precession is solved on the radiation reaction timescale (and then transformed to the frequency domain), which is used to map the nonprecessional waveform from the source frame of the binary to the lab frame. The treatment of orbital precession is different from that for precessional binary black holes, as χ_{eff} is no longer conserved due to the spin-induced quadrupole moments of neutron stars. We show that the new waveform achieves $\leq 10^{-4}$ difference in terms of the one minus the overlap compared with waveforms generated by numerically evolved precession for neutron star-black hole systems for $\geq 90\%$ configurations with component mass/spin magnitude assumed in the analysis and randomized initial spin directions. We expect this waveform to be useful to test the nature of the mass-gap objects similar to the one discovered in GW 190814 by measuring their spin-induced quadrupole moments, as it is possible that these mass-gap objects are rapidly spinning. It is also applicable for the tests of black hole mimickers in precessional binary black hole events, if the black hole mimicker candidates have nontrivial spin-induced quadrupole moments.

DOI: [10.1103/PhysRevD.108.043018](https://doi.org/10.1103/PhysRevD.108.043018)

I. INTRODUCTION

Since the first gravitational wave (GW) observation in 2015, almost a hundred binary coalescences have been detected [1–3], including black hole binaries (BHBH), neutron star binaries (NSNS), and neutron star-black hole binaries (NSBH). In order to distinguish neutron stars from black holes in these binaries, besides information from electromagnetic counterparts, a natural way is to measure the dimensionless tidal deformability ($\Lambda = (2/3)k_2[(c^2/G)(R/M)]^5$) of the compact object [4], which is zero for black holes but could be $\mathcal{O}(10^2\text{--}10^3)$ for normal neutron stars. However, no definite detection of nonzero tidal deformability has been made yet. For example, in the first binary neutron star event detected (GW 170817), the dimensionless tidal deformability is constrained to be ≤ 800 [5,6]. In addition, the tidal deformability decreases sharply with increasing neutron star mass. For heavy

neutron stars near their maximum mass, the corresponding dimensionless tidal deformability is likely only $\mathcal{O}(10)$ [7], which is at best detectable by the third-generation gravitational wave detectors [8]. Without definite information from tidal deformability and electromagnetic counterparts, a common practice is to label compact objects with mass $\leq 3M_\odot$ as neutron stars, and those with mass $\geq 5M_\odot$ as black holes. This is motivated by the lack of black hole observation from x-ray binaries (the “mass-gap”) and neutron star equation-of-state considerations. However, it remains an open question whether there is a detectable population of low-mass black holes (that is, black holes with comparable masses to neutron stars) [9], possibly coming from delayed supernovae explosions, binary neutron star mergers, or primordial black holes. A recent study suggests that they may also take place in extreme mass ratio inspirals suitable for space-borne gravitational wave detections [10], with an accelerated formation rate through the

interaction with accretion disks [11,12]. It is both physically interesting and astrophysically important to unambiguously identify the nature of (at least some of the) mass-gap objects.

The measurement of the spin-induced quadrupole moment may provide a promising method to distinguish neutron stars from low-mass black holes in cases in which this may not be possible otherwise. A key example is GW190814 [13], which describes the coalescence of a $\sim 23M_{\odot}$ black hole with a compact object of $\sim 2.6M_{\odot}$; this compact object may be a low-mass black hole or a heavy neutron star [14–16].¹ With the lighter object lying squarely inside the lower mass gap, an extremely small tidal deformability [expected to be $\leq \mathcal{O}(10)$, below what is likely detectable] and no optical counterpart, it is difficult to determine the identity of this object. A measurement of the spin-induced quadrupole moment from the gravitational waveform could provide insight into the nature of this object, if sufficiently different from that of a black hole. This particular event is especially tantalizing: While neutron stars are not in general expected to have large spins, if this object were a neutron star, it is natural to expect that it would be rapidly spinning in order to support its large mass. On the other hand, if it were a low-mass black hole, large spin is also expected if it is formed in a binary neutron star merger or delayed supernova with significant accretion. This potentially large spin would make the effects of spin precession more pronounced, making it a good candidate for the measurement of the spin-induced quadrupole moment. In particular, we can write the spin-induced quadrupole moment as

$$Q = \kappa a^2 m^3 \quad (1.1)$$

with Q being the magnitude of the quadrupole moment, m its mass, and a its spin. For black holes, the quadrupole constant κ equals 1 (i.e., the Kerr metric), and for neutron stars κ is a (larger-than-one) number depending on the star's mass and equation of state (see Fig. 1 of [7]).

In order to determine the spin-induced quadrupole moment, accurate waveform models are required. There are current waveform models that include the effects of $\kappa \neq 1$, such as TEOBResumS [19] or NRTidal [20]. However, these models only include the effects of $\kappa \neq 1$ on the nonprecessing part of the waveform: The former is a nonprecessing waveform model with the relative precession implemented on top of it, while the latter has precessing waveforms in NRTidalv2, but they do not modify the spin dynamics with contributions from $\kappa \neq 1$. Currently, there are no efficient methods of generating waveforms that include the effects of the spin-induced

quadrupole moment on the precessional dynamics of generic compact objects. Such methods exist for black hole binaries [21–23], but these have not been extended to include the effects of the quadrupole moment of neutron stars. This is the goal of this paper. We solve the spin dynamics component of the waveform; other parts of the waveform generation are then kept the same as nonprecessional systems.

For precessing compact binaries, it is computationally expensive to track the binary evolution on the precession timescale, which is generally longer than the orbital timescale but shorter than the radiation reaction timescale. For binary black hole systems, it has been shown that there are a sufficient number of conserved quantities (in particular, χ_{eff} , as discussed later) such that the spin evolution equation can be solved algebraically after performing an average over the precession timescale [21,22]. However, the quantity χ_{eff} is no longer conserved for generic black hole-neutron star systems as neutron stars have $\kappa \neq 1$, so that the precessional binary black hole waveform no longer applies for binaries with neutron stars, even without considering tidal effects.

The separation of the orbital, precession, and radiation reaction timescales has been used in much of the literature starting with [24] and more recently [25,26]. We will work within the orbit averaged equations, and take advantage of the separation between the precession and radiation reaction (RR) timescales to separate our description into a secular portion (determined by the RR) and a periodic portion (determined by the conservative dynamics). This process requires first solving the conservative problem, so we start by finding an approximate analytic solution to the conservative dynamics. When solving the conservative problem we have three spins each with three components, so that we have nine variables describing the system. For black hole binaries there are seven conserved quantities and two dynamical variables. As mentioned, one of these conserved quantities, χ_{eff} , is no longer conserved when one of the compact objects is not a black hole. This leaves us with a choice when solving the conservative dynamics: either find a new conserved quantity to reduce the problem back to two dynamical variables or work with three dynamical variables.

To decide which is the preferable option we looked at the BHBH case for insight. For black hole binaries, the conservative dynamics have been solved for several different choices of dynamical variables [21,22]. We follow the definitions used in Klein (2021) [22], namely using the sum (χ_{eff}) and difference ($\delta\chi$) of the spins projected onto the orbital angular momentum as two of our three dynamical variables. For this choice, the conservative problem has an exact solution, but this solution relies on the specific form of the evolution equation for $\delta\chi$: Because it is cubic, its roots can be found exactly making the solution efficient. We find that the new conserved quantity in the general case

¹If more exotic objects such as boson stars exist, they may be candidates of mass-gap objects as well with the corresponding tidal deformability potentially measurable [17,18].

is quadratic in both χ_{eff} and $\delta\chi$. This changes the cubic form of $\delta\chi$'s equation so that we can no longer use the techniques that applied previously to solve the system. Thus, while using the conserved quantity directly to reduce the number of dynamical variables may be tempting at first, we opt to continue working with three dynamical variables.

With this choice in mind we find an approximate analytic solution to the conservative dynamics, which can be described in terms of an average, amplitude, and precession phase. The average (secular) portion and amplitude both evolve on the RR timescale. The precession phase obviously evolves on the precession timescale; however, it can be evolved accurately on the RR timescale because the frequency only evolves on the RR timescale. As a result, one can evolve all quantities on the RR timescale, while still fully accounting for the precession.

The organization of the paper is as follows. In Sec. II we lay out the relevant definitions, and in the following section, Sec. III, we lay out the relevant equations. In Sec. IV, we solve the conservative dynamics, and in Sec. V we introduce radiation reaction. In Sec. VI we evaluate the accuracy of this model, and compare the waveform with the binary black hole case to illustrate the phase difference introduced by the spin-induced quadrupole moment.

II. ANGULAR MOMENTA AND SPIN VARIABLES

A note about notation: we will use an arrow \vec{V} to denote vectors, and a hat \hat{V} to denote unit vectors, and merely the symbol itself V to denote the magnitudes. From the total mass $M = m_1 + m_2$, we can define the reduced masses

$$\mu_i = \frac{m_i}{M}. \quad (2.1)$$

From this, it will be useful to define two combinations of the two reduced masses, the first being their difference

$$\delta\mu = \mu_1 - \mu_2, \quad (2.2)$$

which is small in the equal mass limit. The second combination is their product (the symmetric mass ratio)

$$\eta = \mu_1\mu_2. \quad (2.3)$$

The magnitude of the orbital angular momentum can be related to the post-Newtonian (PN) parameter through the symmetric mass ratio

$$L = \frac{\eta}{y}. \quad (2.4)$$

This is one of the conserved quantities of the conservative dynamics. The next quantities of interest are the dimensionless spin parameter

$$\chi_i = \frac{S_i}{m_i^2} \quad (2.5)$$

and the reduced spins

$$\vec{s}_i = \frac{1}{\mu_i} \vec{S}_i. \quad (2.6)$$

The magnitudes of the spins, S_1 and S_2 are two more conserved quantities on the precession timescale. From the reduced spins and the orbital angular momentum, the total angular momentum is defined as

$$\vec{J} = \vec{L} + \mu_1 \vec{s}_1 + \mu_2 \vec{s}_2. \quad (2.7)$$

Its three components form three additional conserved quantities of the conservative dynamics (and consequently its magnitude is another, but it is not unique).

These spins evolve according to the precession equations

$$\begin{aligned} \frac{d\hat{L}}{dt} &= -y^6(\Omega_1 + \Omega_2) \\ \frac{d\vec{s}_1}{dt} &= \mu_2 y^5 \Omega_1 \\ \frac{d\vec{s}_2}{dt} &= \mu_1 y^5 \Omega_2 \end{aligned} \quad (2.8)$$

where

$$\begin{aligned} \Omega_i &= \left\{ \frac{1}{2} \mu_i + \frac{3}{2} [1 - y\hat{L} \cdot (\kappa_i \vec{s}_i + \vec{s}_j)] \right\} \hat{L} \times \vec{s}_i \\ &\quad + \frac{1}{2} y \vec{s}_j \times \vec{s}_i. \end{aligned} \quad (2.9)$$

From these quantities, we denote the sum of the projections of the reduced spins onto the orbital angular momentum as χ_{eff}

$$\chi_{\text{eff}} = \hat{L} \cdot \vec{s}_1 + \hat{L} \cdot \vec{s}_2, \quad (2.10)$$

which is one of the conserved quantities of the binary black-hole (BBH) system first found by [27] and later shown to be conserved by [28] (after orbit averaging, it is not instantaneously conserved). The difference is $\delta\chi$

$$\delta\chi = \hat{L} \cdot \vec{s}_1 - \hat{L} \cdot \vec{s}_2. \quad (2.11)$$

The angle between \hat{L} and \hat{J} is denoted

$$\cos(\theta_L) = \hat{L} \cdot \hat{J}, \quad (2.12)$$

which can also be written in terms of the other projections using Eqs. (2.7)–(2.11),

$$\cos(\theta_L) = \frac{1}{2J} (2L + \chi_{\text{eff}} + \delta\mu\delta\chi). \quad (2.13)$$

III. EQUATIONS OF MOTION

The precession equations for compact objects on circular orbits including leading PN order spin-orbit and spin-spin interactions—without radiation reaction terms—in principle require nine variables for the description: three for the spin of each body and three for the Newtonian angular momentum. At 2.5 post-Newtonian order one can show that there are six straightforward conserved quantities (the magnitudes of each individual angular momentum S_1 , S_2 , and L as well as the three components of the total angular momentum). As a result, we will need three additional variables to complete the description of the angular momenta.

When the two compact objects are black holes, there is in fact an easily identifiable seventh conserved quantity, χ_{eff} , which is a projection of the sum of the reduced spins onto the direction of the Newtonian orbital angular momentum L (see Appendix B for the mathematical expression). This would leave two dynamical quantities to describe the system completely. Previously for the binary black hole scenario, the square of the magnitude of the sum of the spins, S^2 , was chosen as the first dynamical variable, while an angle describing how much the orbital angular momentum has precessed around the total angular momentum, ϕ_z , was chosen as the second [21,25]. Another equivalent choice is to instead use the cosine of the angle between the orbital angular momentum and the total angular momentum, $\cos(\theta_L)$, as the first dynamical variable (keeping ϕ_z as the second). Both choices have the disadvantage that their evolution is singular in the equal mass limit. Klein proposed a different choice for the first dynamical quantity: $\delta\chi$, which is the difference of the projection of the reduced spins. With this choice, the evolution is well defined in the equal mass limit. For this reason this choice is preferred over using S^2 or $\cos(\theta_L)$ and ϕ_z . The relation between these variables and the angular momenta of the individual objects and orbital angular momentum is given in App. II [see also Eqs. (10)–(11) in [22], where a detailed description of their evolution appears].

Here, we extend previous results describing the precession of black holes to other compact objects by including the leading order finite-size effects through the quadrupole moment constants κ_i . κ_i is a coefficient that appears in the quadrupole moment of compact objects, $Q_i = -\kappa_i \chi_i^2 m_i^3$, and is determined by their properties, e.g., the equation of state. For rotating black holes κ is equal to 1. For other compact objects, $\kappa \neq 1$. Specifically, for neutron stars, $\kappa > 1$, and it is larger for stiffer equations of state [29].

For a system where $\kappa_i \neq 1$, χ_{eff} is no longer a conserved quantity. This leaves us with a choice: either find a seventh conserved quantity to reduce the number of dynamical variables back to two, or work with three dynamical variables. While the former option may seem simpler, as we will show in a later section, because of the more complicated form of the conserved quantity it will turn out

to be easier to work with three dynamical variables. Therefore, we use χ_{eff} , $\delta\chi$, and ϕ_z as our set of dynamical variables. As noted in [22], the equations for χ_{eff} and $\delta\chi$ take the form

$$\left(\frac{d\delta\chi}{dt}\right)^2 = \frac{9y^{11}}{4} A_{\delta\chi}^2 (\delta\mu\delta\chi^3 + B\delta\chi^2 + C\delta\chi + D) \quad (3.1)$$

and

$$\left(\frac{d\chi_{\text{eff}}}{dt}\right)^2 = \frac{9y^{11}}{4} A_{\chi_{\text{eff}}}^2 (\delta\mu\delta\chi^3 + B\delta\chi^2 + C\delta\chi + D), \quad (3.2)$$

where

$$\begin{aligned} A_{\delta\chi} &= 1 + yA_{\delta\chi,\delta\chi}\delta\chi + yA_{\delta\chi,\chi_{\text{eff}}}\chi_{\text{eff}}, \\ A_{\chi_{\text{eff}}} &= yA_{\chi_{\text{eff}},\delta\chi}\delta\chi + yA_{\chi_{\text{eff}},\chi_{\text{eff}}}\chi_{\text{eff}}, \end{aligned} \quad (3.3)$$

with y a PN parameter related to the norm of the orbital angular momentum [in particular, $y = (M\omega)^{\frac{1}{3}}$ with M the total mass, and ω the mean orbital frequency]. The coefficients B , C , and D depend on the conserved quantities, the PN parameter, and χ_{eff} , and are given in Appendix B (see also [22] [Appendix B]). The coefficients in A are

$$A_{\delta\chi,\delta\chi} = \frac{\kappa_2 - \kappa_1}{4}, \quad (3.4a)$$

$$A_{\delta\chi,\chi_{\text{eff}}} = -\frac{\kappa_1 + \kappa_2 + 2}{4}, \quad (3.4b)$$

$$A_{\chi_{\text{eff}},\delta\chi} = \frac{\kappa_1 + \kappa_2 - 2}{4}, \quad (3.4c)$$

$$A_{\chi_{\text{eff}},\chi_{\text{eff}}} = \frac{\kappa_1 - \kappa_2}{4}. \quad (3.4d)$$

When $\kappa_i = 1$, the equations reduce to those in [22]. To solve the dynamical equations, we will separate the behavior of χ_{eff} and $\delta\chi$ in the next section.

The amount the orbital angular momentum has precessed around the total angular momentum ϕ_z evolves according to

$$\frac{d\phi_z}{dt} = \frac{1}{\sin^2(\theta_L)} \left[\frac{d\hat{L}}{dt} \cdot (\hat{J} \times \hat{L}) \right], \quad (3.5)$$

where θ_L is the angle between the orbital angular momentum and the total angular momentum, and the hats on the orbital angular momentum L and total angular momentum J indicate that these are the direction vectors in the directions of the corresponding angular momentum. While ϕ_z has a nice physical interpretation, it will also be useful to define a related angle ζ , used in waveform generation [21]

$$\frac{d\zeta}{dt} = -\cos(\theta_L) \frac{d\phi_z}{dt}. \quad (3.6)$$

Once we include radiative effects, we need to take into account that the conserved quantities are no longer constant. The radiation reaction behavior is determined, largely, by two things, dy/dt and dJ/dt , the latter of which is given by [22]:

$$\frac{dJ}{dt} = -\frac{L}{2Jy} \frac{dy}{dt} (2L + \chi_{\text{eff}} + \delta\mu\delta\chi), \quad (3.7)$$

where $\delta\mu$ is the difference of the reduced masses $\delta\mu = \mu_1 - \mu_2$.

IV. ANALYTIC SOLUTION TO THE PRECESSION WITHOUT RADIATION REACTION

To solve the equations describing inspiraling precessing black hole or neutron star binaries on circular orbits, we take advantage of the fact that an (approximate) analytic solution exists for the conservative problem, as we will show in this section. In Sec. V, we include the effects of radiation reaction. To determine the conservative evolution, we separate the problem into a secular and a periodic part. The secular part of the solution is constant for $\delta\chi$, χ_{eff} , and J without considering radiation reaction. In contrast, the remaining key quantities, that is, ϕ_z and ζ , have a secular part that evolves even in the absence of radiation reaction. As such, for the former quantities, it is satisfactory to focus only on their periodic parts. The evolution of the angles ϕ_z and ζ requires additional treatment. Therefore, we start by examining the periodic part of $\delta\chi$ and χ_{eff} , before we discuss the more involved cases of ϕ_z and ζ .

As mentioned, in the black hole binary case (for which $\kappa_1 = \kappa_2 = 1$), the effective spin χ_{eff} is a constant of the conservative dynamics. This makes the process for solving the equation for $\delta\chi$ straightforward. In particular, the coefficients in the equation for $\delta\chi$ in Eq. (3.1) are all constant so that $\delta\chi$ oscillates between its minimum and maximum values, $\delta\chi_-$ and $\delta\chi_+$, respectively. The solution is then easily obtained by treating the solution as an average and oscillatory part, with $\delta\chi_-$ and $\delta\chi_+$ determining the average part of the solution as well as the amplitude of the oscillatory part. One is then only left to evolve the phase of the oscillatory part.

If one or both objects in the binary are neutron stars so that $\kappa_i \neq 1$, χ_{eff} becomes dynamical and oscillates. As a result, the coefficients B , C , and D appearing in Eqs. (3.1) and (3.2) are now dynamical and so are its minima and maxima, $\delta\chi_-$ and $\delta\chi_+$. We overcome this complication by deriving an approximate linear relation between $\delta\chi$ and χ_{eff} , so that χ_{eff} can be replaced by $\delta\chi$ in Eq. (3.1), and the resulting equation for $\delta\chi$ becomes independent of χ_{eff} . Consequently, the roots on the right-hand side of Eq. (3.1) again correspond to the true maximum and minimum of $\delta\chi$.

This allows us to solve for the dynamics of $\delta\chi$. Then, using the linear relation between $\delta\chi$ and χ_{eff} , the evolution of χ_{eff} is trivially obtained.

In the remainder of this section, we first derive this important linear relation in two different ways in Sec. IV A and IV B. Next, we solve for the dynamics of $\delta\chi$ and χ_{eff} in Secs. IV C–IV E. In Sec. IV F, we discuss the dynamics for ϕ_z and ζ .

A. Approximate relation between $\delta\chi$ and χ_{eff}

If the coefficients in Eq. (3.1) are constant, as is the case when both objects in the binary are black holes, the *exact* solution to this equation is given by the Jacobi elliptic function

$$\delta\chi(t) = \delta\chi_- + (\delta\chi_+ - \delta\chi_-) \text{sn}^2(\psi'(t), m), \quad (4.1)$$

where ψ' describes the phase evolution of the precession and the parameter $m = \delta\mu(\delta\chi_+ - \delta\chi_-)/(\delta\chi_3 - \delta\mu\delta\chi_-)$ with $\delta\chi_3$ containing information of the largest root of the cubic equation on the right-hand side of Eq. (3.1) [see Eq. (4.22)]. In the limit $m \rightarrow 0$, the Jacobi elliptic function reduces to the usual sine function. We will use this insight to approximate the solutions for $\delta\chi$ and χ_{eff} in the generic case for which $\kappa_i \neq 1$ as

$$\begin{aligned} \delta\chi &\approx \langle \delta\chi \rangle + G_{\delta\chi} \sin(\psi), \\ \chi_{\text{eff}} &\approx \langle \chi_{\text{eff}} \rangle + G_{\chi_{\text{eff}}} \sin(\psi), \end{aligned} \quad (4.2)$$

where

$$\begin{aligned} \langle \delta\chi \rangle &= \frac{1}{2}(\delta\chi_+ + \delta\chi_-), \\ G_{\delta\chi} &= \frac{1}{2}(\delta\chi_+ - \delta\chi_-), \\ \langle \chi_{\text{eff}} \rangle &= \frac{1}{2}(\chi_{\text{eff},+} + \chi_{\text{eff},-}), \\ G_{\chi_{\text{eff}}} &= \frac{1}{2}(\chi_{\text{eff},+} - \chi_{\text{eff},-}). \end{aligned} \quad (4.3)$$

Here we have used the brackets to indicate that there is some time average underlying these expressions; indeed the first expression corresponds to the actual precession average of $\delta\chi$ in Eq. (4.1) in the $m \rightarrow 0$ limit. This precession average is performed on the precession timescale, $T_{pr} \sim O(y^{-5})$ which corresponds to the rate at which the precession phase, ψ , evolves. This is in contrast to the radiation reaction timescale, $T_{rr} \sim O(y^{-8})$, on which the entire evolution occurs. This separation of scales allows one to disregard the changes in these quantities during the precession averaging when adding radiation reaction.

In these approximate expressions, we have used ψ instead of ψ' that appears in the original expressions, because we have simplified the \sin^2 term using the half

angle formula and identified $2\psi' = \psi + \pi/2$ so that the final expression is expressible in terms of a sine function again. This simple form of the solution matches well with numerical evolutions of the coupled equations. Moreover, this form is very powerful as it will allow us to relate $\delta\chi$ and χ_{eff} . Note that due to the similarity in their derivatives in Eqs. (3.1) and (3.2), when one solution has reached its extrema the other must have as well. This is the reason why both solutions oscillate with a single phase ψ . In analogy to the solutions in [21,22], we will refer to the ansatz in Eq. (4.2) as the “ $m = 0$ ” approximation.

Operating within this approximation, Eqs. (3.1) and (3.2) can be related to obtain

$$A_{\chi_{\text{eff}}}^2 \left(\frac{d\delta\chi}{dt} \right)^2 = A_{\delta\chi}^2 \left(\frac{d\chi_{\text{eff}}}{dt} \right)^2. \quad (4.4)$$

Substituting the approximate definitions (4.2) into the above relation then gives

$$\begin{aligned} & (yA_{\chi_{\text{eff}},\delta\chi}\delta\chi + yA_{\chi_{\text{eff}},\chi_{\text{eff}}}\chi_{\text{eff}})^2 G_{\delta\chi}^2 \\ &= (1 + yA_{\delta\chi,\delta\chi}\delta\chi + yA_{\delta\chi,\chi_{\text{eff}}}\chi_{\text{eff}})^2 G_{\chi_{\text{eff}}}^2. \end{aligned} \quad (4.5)$$

Evaluating this at $\psi = 0$ relates the amplitude of one quantity, $G_{\chi_{\text{eff}}}$, to the amplitude of the other, $G_{\delta\chi}$:²

$$\left| \frac{G_{\chi_{\text{eff}}}}{G_{\delta\chi}} \right| = \left| \frac{yA_{\chi_{\text{eff}},\delta\chi}\langle\delta\chi\rangle + yA_{\chi_{\text{eff}},\chi_{\text{eff}}}\langle\chi_{\text{eff}}\rangle}{1 + yA_{\delta\chi,\delta\chi}\langle\delta\chi\rangle + yA_{\delta\chi,\chi_{\text{eff}}}\langle\chi_{\text{eff}}\rangle} \right|. \quad (4.6)$$

Next, solving for $\sin(\psi)$ in (4.2), we obtain the desired relation between χ_{eff} and $\delta\chi$:

$$\chi_{\text{eff}} = \langle\chi_{\text{eff}}\rangle - \frac{G_{\chi_{\text{eff}}}}{G_{\delta\chi}} \langle\delta\chi\rangle + \frac{G_{\chi_{\text{eff}}}}{G_{\delta\chi}} \delta\chi. \quad (4.7)$$

Having already found the relation between the amplitudes $G_{\chi_{\text{eff}}}/G_{\delta\chi}$ in terms of the averages, this equation is entirely determined so long as the average values of χ_{eff} and $\delta\chi$ are known. Thus the desired result is achieved: an approximate linear relation in the absence of radiation reaction between $\delta\chi$ and χ_{eff} defined by their averages (which are known constants). This relation will be used in Sec. IV D to obtain a new dynamical equation for $\delta\chi$ that no longer depends on the dynamics of χ_{eff} but only on its average and amplitude.

B. Another perspective: The amplitude relation from a conserved quantity

The relation between χ_{eff} and $\delta\chi$ in (4.7) holds approximately because it was derived assuming that the solutions for χ_{eff} and $\delta\chi$ have the simple form given in Eq. (4.2). Here, we show that the amplitude relation in Eq. (4.6) holds more generically as long as the average/amplitude of χ_{eff}

²Note that the inverse of this expression is not well defined in the black hole limit.

and $\delta\chi$ can be understood purely as a sum/difference between the maxima and minima.

Starting with (3.1) and (3.2), the chain rule gives

$$\left(\frac{d\chi_{\text{eff}}}{d\delta\chi} \right)^2 = \left(\frac{yA_{\chi_{\text{eff}},\delta\chi}\delta\chi + yA_{\chi_{\text{eff}},\chi_{\text{eff}}}\chi_{\text{eff}}}{1 + yA_{\delta\chi,\delta\chi}\delta\chi + yA_{\delta\chi,\chi_{\text{eff}}}\chi_{\text{eff}}} \right)^2. \quad (4.8)$$

Let us first discuss the special case with $A_{\chi_{\text{eff}},\chi_{\text{eff}}} = 0 = A_{\delta\chi,\delta\chi}$ for which one directly obtains a solution through its quadratures

$$\begin{aligned} & 1 + yA_{\delta\chi,\chi_{\text{eff}}}\chi_{\text{eff}} \\ &= \sqrt{1 + A_{\chi_{\text{eff}},\delta\chi}A_{\delta\chi,\chi_{\text{eff}}}y^2(c_1\delta\chi^2 + c_2)}, \end{aligned} \quad (4.9)$$

where $c_1 = \pm 1$ arises from a choice of sign when taking the square root of (4.8), and c_2 is a constant of integration. Squaring both sides gives

$$\begin{aligned} & 2yA_{\delta\chi,\chi_{\text{eff}}}\chi_{\text{eff}} + y^2A_{\delta\chi,\chi_{\text{eff}}}^2\chi_{\text{eff}}^2 \\ &= A_{\chi_{\text{eff}},\delta\chi}A_{\delta\chi,\chi_{\text{eff}}}y^2(c_1\delta\chi^2 + c_2). \end{aligned} \quad (4.10)$$

While (4.2) is an approximate relation for generic values of ψ , by definition of the average and amplitudes in (4.3), Eq. (4.2) holds exactly when $\psi = \pm\pi/2$. As a result, we can substitute Eq. (4.2) evaluated at $\psi = \pi/2$ into (4.10) without loss of generality. Subtracting off the same equation evaluated at $\psi = -\pi/2$ gives

$$\left| \frac{G_{\chi_{\text{eff}}}}{G_{\delta\chi}} \right| = \left| \frac{yA_{\chi_{\text{eff}},\delta\chi}\langle\delta\chi\rangle}{1 + yA_{\delta\chi,\chi_{\text{eff}}}\langle\chi_{\text{eff}}\rangle} \right|, \quad (4.11)$$

where the factor of c_1 has been replaced in favor of expressing this as a relation in terms of the magnitudes of the amplitudes. This equation recovers the result in Eq. (4.6) for the case at hand: $A_{\chi_{\text{eff}},\chi_{\text{eff}}} = 0 = A_{\delta\chi,\delta\chi}$.

The general case in which $A_{\chi_{\text{eff}},\chi_{\text{eff}}} \neq 0$ and $A_{\delta\chi,\delta\chi} \neq 0$ is obtained in the same manner. Specifically, by making the substitution

$$\begin{aligned} Z &= \chi_{\text{eff}} - A_{\chi_{\text{eff}},\delta\chi}/y(A_{\delta\chi,\delta\chi}A_{\chi_{\text{eff}},\chi_{\text{eff}}} - A_{\chi_{\text{eff}},\delta\chi}A_{\delta\chi,\chi_{\text{eff}}}) \\ X &= \delta\chi + A_{\chi_{\text{eff}},\chi_{\text{eff}}}/y(A_{\delta\chi,\delta\chi}A_{\chi_{\text{eff}},\chi_{\text{eff}}} - A_{\chi_{\text{eff}},\delta\chi}A_{\delta\chi,\chi_{\text{eff}}}), \end{aligned} \quad (4.12)$$

and using the chain rule, we find

$$\frac{dZ}{dX} = \frac{A_{\chi_{\text{eff}},\delta\chi}X + A_{\chi_{\text{eff}},\chi_{\text{eff}}}Z}{A_{\delta\chi,\delta\chi}X + A_{\delta\chi,\chi_{\text{eff}}}Z}. \quad (4.13)$$

The solution to this equation is implicitly given by

$$4(A_{\delta\chi,\chi_{\text{eff}}}Z + A_{\delta\chi,\delta\chi}X)^2 = -(\kappa_1\kappa_2 - 1)X^2 + c_2, \quad (4.14)$$

where we have again denoted the constant of integration corresponding to the conserved quantity as c_2 , to highlight that it arises in a manner similar to Eq. (4.10). Again, evaluating this expression using (4.2) at $\psi = \pi/2$ and

subtracting off the same equation evaluated at $\psi = -\pi/2$, one finds the amplitude relation in Eq. (4.6).

As alluded to before, Eq. (4.14) points to a conserved quantity in the case with $\kappa_i \neq 1$. In the black hole case, this conserved quantity was simply χ_{eff} , but here it is nonlinear in $\delta\chi$ and χ_{eff} . Of course, in the limit $\kappa_i = 1$, this equation simply states that χ_{eff} is conserved. In Eq. (4.10) this limit is slightly more obvious; $A_{\chi_{\text{eff}}, \delta\chi} = 0$ in this limit, and (after absorbing other conserved quantities into our definition) we find that χ_{eff} is conserved.

While the existence of this conserved quantity would reduce the number of dynamic quantities from three to two, it is more useful to use the approximate linear relation instead. This is because the linear relation maintains the cubic nature of Eq. (3.1) in terms of $\delta\chi$, meaning its roots can be found analytically. If instead the exact relation in Eq. (4.10) were used, it would make the roots of the equation too difficult to find analytically. Numerical root finding would make this method impractical computationally, for little benefit in accuracy.

C. Finding the initial averages of $\delta\chi$ and χ_{eff}

In order to calculate the amplitudes of $\delta\chi$ and χ_{eff} , from Eqs. (4.6) and (4.7), it is clear that we need to know their average values. Consequently, the averages need to be calculated from known quantities (such as J , y , and the initial values of χ_{eff} and $\delta\chi$). To do this, first we compute the numerical value of the first three derivatives for the initial values of χ_{eff} and $\delta\chi$, evaluated using Eq. (3.1). We then relate these values to the first three derivatives of the approximate relation Eq. (4.2), given as

$$\begin{aligned} \frac{d\delta\chi}{dt} &\approx \frac{d\psi}{dt} G_{\delta\chi} \cos(\psi), \\ \frac{d^2\delta\chi}{dt^2} &\approx -\left(\frac{d\psi}{dt}\right)^2 G_{\delta\chi} \sin(\psi), \\ \frac{d^3\delta\chi}{dt^3} &\approx -\left(\frac{d\psi}{dt}\right)^3 G_{\delta\chi} \cos(\psi), \end{aligned} \quad (4.15)$$

where here we have not included the second and third derivatives of ψ because they are zero in the absence of radiation reaction. In the presence of radiation reaction they are not zero, but as a result of multiscale analysis they correspond to the evolution of ψ on the radiation reaction timescale, and as a result their noninclusion does not produce significant error. We then solve the ensuing system of equations to obtain

$$\begin{aligned} \langle \delta\chi \rangle &\approx \delta\chi - \delta\chi'' \delta\chi / \delta\chi''', \\ \tan(\psi) &\approx |(\delta\chi'' / \delta\chi''') \sqrt{-\delta\chi''' / \delta\chi'}|, \\ \left| \frac{d\psi}{dt} \right| &\approx \sqrt{-\delta\chi''' / \delta\chi'}, \\ |G_{\delta\chi}| &\approx \sqrt{(\delta\chi')^2 / (d\psi/dt)^2 + (\delta\chi'')^2 / (d\psi/dt)^4}, \end{aligned} \quad (4.16)$$

where the second equation is true up to a factor of π and a plus or minus sign depending on the signs of the initial derivatives; to get around this we define the phase in such a way that the amplitude of $\delta\chi$ is always positive. Since we are working in the conservative dynamics currently, the average, initial amplitude, and precession frequency are constant; when we include radiation reaction these will also evolve, the description of which is given later.

D. Finding the amplitudes of $\delta\chi$ and χ_{eff}

Now, with the averages in hand, the relation (4.7) can be used to find the amplitudes. To simplify the next set of calculations we define

$$\chi_{\text{eff}} = N_0 + N_1 \delta\chi, \quad (4.17)$$

where [as a result of (4.7)] these coefficients are given by

$$\begin{aligned} N_0 &= \langle \chi_{\text{eff}} \rangle - \frac{G_{\chi_{\text{eff}}}}{G_{\delta\chi}} \langle \delta\chi \rangle, \\ N_1 &= \frac{G_{\chi_{\text{eff}}}}{G_{\delta\chi}}. \end{aligned} \quad (4.18)$$

Substituting this into (3.1) gives a new equation of the form

$$\left(\frac{d\delta\chi}{dt} \right)^2 = \frac{9y^{11}}{4} A_{\delta\chi}^2 (X_3 \delta\chi^3 + X_2 \delta\chi^2 + X_1 \delta\chi + X_0), \quad (4.19)$$

where

$$\begin{aligned} X_0 &= D_3 N_0^3 + D_2 N_0^2 + D_1 N_0 + D_0, \\ X_1 &= 3D_3 N_0^2 N_1 + C_2 N_0^2 + 2D_2 N_0 N_1 + C_1 N_0 + D_1 N_1 + C_0, \\ X_2 &= 3D_3 N_0 N_1^2 + 2C_2 N_0 N_1 + D_2 N_1^2 + B_1 N_0 + C_1 N_1 + B_0, \\ X_3 &= D_3 N_1^3 + C_2 N_1^2 + B_1 N_1 + \delta\mu. \end{aligned} \quad (4.20)$$

In the above expression, we have organized the coefficients of B , C , and D that appear in Eq. (3.1) in the following way:

$$\begin{aligned} B &= B_0 + B_1 \chi_{\text{eff}}, \\ C &= C_0 + C_1 \chi_{\text{eff}} + C_2 \chi_{\text{eff}}^2, \\ D &= D_0 + D_1 \chi_{\text{eff}} + D_2 \chi_{\text{eff}}^2 + D_3 \chi_{\text{eff}}^3. \end{aligned} \quad (4.21)$$

The explicit form of these coefficients is given in Appendix B. As discussed, because this cubic no longer implicates χ_{eff} , the roots are now the true maximum and minimum values of $\delta\chi$, $\delta\chi_+$, and $\delta\chi_-$. The amplitude of the oscillatory part of $\delta\chi$ is then obtained via its definition $G_{\delta\chi} = \frac{1}{2}(\delta\chi_+ - \delta\chi_-)$. Finally, Eq. (4.7) can then be used to find the amplitude for χ_{eff} .

E. Evolving the phase of $\delta\chi$ and χ_{eff}

With both the averages and amplitudes of $\delta\chi$ and χ_{eff} in hand, we are only left to determine the evolution of the phase ψ . For reference we re-express the relevant derivative, Eq. (4.19), in the most immediately useful form:

$$\left(\frac{d\delta\chi}{dt}\right)^2 = \frac{9y^{11}}{4} X_3 A_{\delta\chi}^2 (\delta\chi - \delta\chi_+) (\delta\chi - \delta\chi_-) \left(\delta\chi - \frac{\delta\chi_3}{\delta\mu}\right), \quad (4.22)$$

where the roots of the cubic equation are ordered such that $\delta\chi_- \leq \delta\chi_+ \leq \delta\chi_3/\delta\mu$. To get an expression for the phase evolution ψ , we substitute Eq. (4.2) into the equation above and use the definition in Eq. (4.4) to simplify the expression. The resulting equation is

$$\left(\frac{d\psi}{dt}\right)^2 = \frac{9y^{11}}{4} X_3 A_{\delta\chi}^2 \left(\frac{\delta\chi_3}{\delta\mu} - \langle\delta\chi\rangle - G_{\delta\chi} \sin(\psi)\right). \quad (4.23)$$

This relation is not approximate; all of the nonlinearity in the original equation is accounted for. Instead of this exact result, it is preferable to use an averaged version

of this equation so that the phase evolves at a fixed rate. Intuitively, the times at which the phase would have evolved faster/slower than its average rate correspond to neglected higher order modes in its Fourier series. [One could include these higher order modes in the definition in (4.2) to account for this; we will not do that here.] To simplify the final expression of this average we first define

$$\begin{aligned} \langle A_{\delta\chi} \rangle &= 1 + y A_{\delta\chi, \delta\chi} \langle \delta\chi \rangle + y A_{\delta\chi, \chi_{\text{eff}}} \langle \chi_{\text{eff}} \rangle, \\ G_A &= y A_{\delta\chi, \delta\chi} G_{\delta\chi} + y A_{\delta\chi, \chi_{\text{eff}}} G_{\chi_{\text{eff}}}. \end{aligned} \quad (4.24)$$

The average rate of change of ψ is then given by

$$\begin{aligned} \left(\frac{d\psi}{dt}\right)^2 &\approx \frac{9y^{11}}{8} X_3 (\delta\chi_3/\delta\mu - \langle\delta\chi\rangle) (2\langle A_{\delta\chi} \rangle^2 + G_A^2) \\ &\quad - G_{\delta\chi} G_A \langle A_{\delta\chi} \rangle. \end{aligned} \quad (4.25)$$

In the absence of radiation reaction, all quantities in the right-hand side are constant, and thus this can be integrated exactly to give

$$\psi(t) \approx \frac{3y^{11/2}}{2^{3/2}} \sqrt{X_3 (\delta\chi_3/\delta\mu - \langle\delta\chi\rangle) (2\langle A_{\delta\chi} \rangle^2 + G_A^2) - G_{\delta\chi} G_A \langle A_{\delta\chi} \rangle} t + \psi(0). \quad (4.26)$$

F. Evolving ϕ_z and ζ

Given χ and χ_{eff} , we now turn to the slightly more complicated evolutions of ϕ_z and ζ as these variables have both an evolving periodic and an evolving secular part, also in the absence of radiation. The derivative of ϕ_z can be given approximately as (see Appendix B)

$$\frac{d\phi_z}{dt} \approx \frac{Jy^6}{2} \left\{ Q_4 + Q_5 \sin(\psi) + \frac{H_0 + H_1 \sin(\psi) + H_2 \sin^2(\psi) + H_3 \sin^3(\psi)}{(1 + H_- \sin(\psi))(1 + H_+ \sin(\psi))} \right\}. \quad (4.27)$$

While this can be integrated exactly, it is useful to split ϕ_z into its secular and periodic part. To do this, we rewrite the derivative of ϕ_z to separate terms with differing behavior:

$$\begin{aligned} \frac{d\phi_z}{dt} &\approx \frac{Jy^6}{2} \left\{ Q_4 + \frac{H_2 H_+ H_- - H_3 H_- - H_3 H_+}{H_+^2 H_-^2} \right\} + \frac{Jy^6}{2} \left\{ Q_5 + \frac{H_3}{H_+ H_-} \right\} \sin(\psi) \\ &\quad + \frac{Jy^6}{2} \left\{ \frac{H_0 H_+^3 - H_1 H_+^2 + H_2 H_+ - H_3}{(H_+ - H_-) H_+^2 (1 + H_+ \sin(\psi))} \right\} - \frac{Jy^6}{2} \left\{ \frac{H_0 H_-^3 - H_1 H_-^2 + H_2 H_- - H_3}{(H_+ - H_-) H_-^2 (1 + H_- \sin(\psi))} \right\}. \end{aligned} \quad (4.28)$$

The first term is purely secular, the second term is purely periodic, and the last two terms are mixed. To split the last two terms into secular and periodic parts, we precession average these terms. The precession average then contributes to the secular part, while the remaining part contributes to the periodic behavior. The resulting secular part is

$$\frac{d\langle\phi_z\rangle}{dt} \approx \Phi_0 + \Phi_+ + \Phi_-, \quad (4.29)$$

and the periodic part is

$$\frac{d\phi_z}{dt} - \frac{d\langle\phi_z\rangle}{dt} \approx \Phi_s \sin(\psi) + \Phi_+ \left(\frac{\sqrt{1-H_+^2}}{1+H_+ \sin(\psi)} - 1 \right) + \Phi_- \left(\frac{\sqrt{1-H_-^2}}{1+H_- \sin(\psi)} - 1 \right), \quad (4.30)$$

where Φ_0 , Φ_s , Φ_+ , and Φ_- are independent of ϕ_z and ζ and defined in Appendix B. The periodic part can be integrated exactly to yield

$$\begin{aligned} \phi_z - \langle\phi_z\rangle \approx & -\frac{\Phi_s}{\dot{\psi}} \cos(\psi) + \frac{\Phi_+}{\dot{\psi}} \left(2 \arctan \left(\frac{\tan(\psi/2) + H_+}{\sqrt{1-H_+^2}} \right) - \psi - \arcsin(H_+) \right) \\ & + \frac{\Phi_-}{\dot{\psi}} \left(2 \arctan \left(\frac{\tan(\psi/2) + H_-}{\sqrt{1-H_-^2}} \right) - \psi - \arcsin(H_-) \right). \end{aligned} \quad (4.31)$$

The constant terms (involving arcsin) come from the constant of integration, and are used to ensure that the average of the periodic part is zero.

The evolution for ζ is solved in a similar manner. Its derivative is given by $d\zeta/dt = -\cos(\theta_L)d\phi_z/dt$. Substituting Eq. (4.28) and the expression for $\cos(\theta_L)$ gives

$$\frac{d\zeta}{dt} \approx -(\Theta_0 + \Theta_s \sin(\psi)) \left(\Phi_0 + \Phi_s \sin(\psi) + \frac{\Phi_+ \sqrt{1-H_+^2}}{1+H_+ \sin(\psi)} + \frac{\Phi_- \sqrt{1-H_-^2}}{1+H_- \sin(\psi)} \right). \quad (4.32)$$

Splitting this into a secular and periodic part, we find that the secular part is

$$\frac{d\langle\zeta\rangle}{dt} \approx -\Theta_0(\Phi_0 + \Phi_+ + \Phi_-) - \frac{\Theta_s \Phi_s}{2} - \frac{\Theta_s \Phi_+}{H_+} \left(\sqrt{1-H_+^2} - 1 \right) - \frac{\Theta_s \Phi_-}{H_-} \left(\sqrt{1-H_-^2} - 1 \right), \quad (4.33)$$

and the periodic part is

$$\begin{aligned} \frac{d\zeta}{dt} - \frac{d\langle\zeta\rangle}{dt} \approx & -\Theta_0 \left(\frac{d\phi_z}{dt} - \frac{d\langle\phi_z\rangle}{dt} \right) - \Theta_s \Phi_0 \sin(\psi) + \frac{\Theta_s \Phi_s}{2} \cos(2\psi) \\ & + \frac{\Theta_s \Phi_+}{H_+} \left(\frac{\sqrt{1-H_+^2}}{1+H_+ \sin(\psi)} - 1 \right) + \frac{\Theta_s \Phi_-}{H_-} \left(\frac{\sqrt{1-H_-^2}}{1+H_- \sin(\psi)} - 1 \right). \end{aligned} \quad (4.34)$$

The periodic part can be integrated exactly to yield

$$\begin{aligned} \zeta - \langle\zeta\rangle \approx & -\Theta_0(\phi_z - \langle\phi_z\rangle) - \frac{\Theta_s \Phi_0}{\dot{\psi}} \cos(\psi) + \frac{\Theta_s \Phi_s}{4\dot{\psi}} \sin(2\psi) + \frac{\Theta_s \Phi_+}{H_+} \left(2 \arctan \left(\frac{\tan(\psi/2) + H_+}{\sqrt{1-H_+^2}} \right) - \psi - \arcsin(H_+) \right) \\ & + \frac{\Theta_s \Phi_-}{H_-} \left(2 \arctan \left(\frac{\tan(\psi/2) + H_-}{\sqrt{1-H_-^2}} \right) - \psi - \arcsin(H_-) \right). \end{aligned} \quad (4.35)$$

V. ADDING RADIATION REACTION

We have discussed the complete conservative dynamics of spins in Sec. IV. With gravitational radiation reaction included, the orbital frequency increases as a function of time, which can be obtained as an expansion in Post-Newtonian orders. The total angular momentum J and the average part of χ_{eff} , $\delta\chi$ become time dependent, with corresponding evolution equations discussed below. We do not discuss the evolution of the secular part of ϕ_z and ζ here as the previous expressions for their derivatives can simply be evaluated and evolved on the radiation reaction

timescale, but with updated values for the averages of J , $\delta\chi$, and χ_{eff} at each step.

A. Evolving J

Restating it here for simplicity, the radiation reaction equation for J is

$$\frac{dJ}{dt} = \frac{-L}{2Jy} \frac{dy}{dt} (2L + \delta\mu\delta\chi + \chi_{\text{eff}}). \quad (5.1)$$

Similarly to before, this can be expressed in the “ $m = 0$ ” approximation, expanding the solution into a secular part

and periodic part. Here, the solution is slightly out of phase with $\delta\chi/\chi_{\text{eff}}$, so an additional term will be required to account for this. Thus, the solution for J should take the following form:

$$J \approx \langle J \rangle + G_{J,s} \sin(\psi) + G_{J,c} \cos(\psi), \quad (5.2)$$

and we are left to determine $\langle J \rangle$, $G_{J,s}$, and $G_{J,c}$. Because the secular part is much smaller than the periodic part, $G_{J,s}/\langle J \rangle$ and $G_{J,c}/\langle J \rangle$ are assumed to be small. Substituting Eqs. (4.2) and (5.2) into Eq. (6.2) and applying this approximation gives

$$\begin{aligned} \frac{d\langle J \rangle}{dt} + G_{J,s} \frac{d\psi}{dt} \cos(\psi) - G_{J,c} \frac{d\psi}{dt} \sin(\psi) \\ \approx \frac{-L}{2\langle J \rangle y} \frac{dy}{dt} (2L + \delta\mu\delta\chi + \chi_{\text{eff}}) \\ + \frac{L}{2\langle J \rangle^2 y} \frac{dy}{dt} (2L + \delta\mu\delta\chi + \chi_{\text{eff}}) \\ \times (G_{J,s} \sin(\psi) + G_{J,c} \cos(\psi)). \end{aligned} \quad (5.3)$$

$d\langle J \rangle/dt$ is found by averaging both sides of this equation with respect to ψ over one cycle:

$$\begin{aligned} \frac{d\langle J \rangle}{dt} = \frac{-L}{2\langle J \rangle y} \frac{dy}{dt} (2L + \delta\mu\langle\delta\chi\rangle + \langle\chi_{\text{eff}}\rangle) \\ + \frac{L}{4\langle J \rangle^2 y} \frac{dy}{dt} G_{J,s} (\delta\mu G_{\delta\chi} + G_{\chi_{\text{eff}}}), \end{aligned} \quad (5.4)$$

where we have treated $d\psi/dt$ as a constant for the purpose of the precession average, because it only evolves on the radiation reaction timescale. Another, alternative way of thinking about this is that the correction to this equation resulting from accounting for the change in $d\psi/dt$ will always be multiplied by one of the two amplitudes of J ; this correction being small and the amplitudes of J also being small means the resulting term is sufficiently small so that it can safely be neglected. A system of equations for $G_{J,s}$ and $G_{J,c}$ can be obtained by multiplying by either $\sin(\psi)$ or $\cos(\psi)$ and averaging over ψ :

$$G_{J,s} \frac{d\psi}{dt} = \frac{L}{2\langle J \rangle^2 y} \frac{dy}{dt} G_{J,c} (2L + \delta\mu\langle\delta\chi\rangle + \langle\chi_{\text{eff}}\rangle) \quad (5.5)$$

$$\begin{aligned} -G_{J,c} \frac{d\psi}{dt} = \frac{-L}{2\langle J \rangle y} \frac{dy}{dt} (\delta\mu G_{\delta\chi} + G_{\chi_{\text{eff}}}) \\ + \frac{L}{2\langle J \rangle^2 y} \frac{dy}{dt} G_{J,s} (2L + \delta\mu\langle\delta\chi\rangle + \langle\chi_{\text{eff}}\rangle). \end{aligned} \quad (5.6)$$

Equations (5.4)–(5.6) form a system of equations for the desired unknowns: $d\langle J \rangle/dt$, $G_{J,s}$, and $G_{J,c}$. In previous works [21,22] the value of J is then used to calculate the roots of $\delta\chi$; instead here we use this derivative of the

average of J to find the derivatives of the averages of $\delta\chi$ and χ_{eff} .

B. Evolving $\langle\delta\chi\rangle$ and $\langle\chi_{\text{eff}}\rangle$

After using the results of Sec. IV C we can obtain the averages $\langle\delta\chi\rangle$ and $\langle\chi_{\text{eff}}\rangle$ at the initial time. In the presence of radiation reaction we must then evolve these averages. First we evolve the roots ($\delta\chi_+$, $\delta\chi_-$, $\chi_{\text{eff},+}$, $\chi_{\text{eff},-}$) and then use the relation between these roots and the averages [Eq. (4.3)] to evolve the averages. To find these derivatives, we start with their definitions as the roots of the following equations:

$$\begin{aligned} \delta\mu\delta\chi_+^3 + (B_0 + B_1\chi_{\text{eff},+})\delta\chi_+^2 \\ + (C_0 + C_1\chi_{\text{eff},+} + C_2\chi_{\text{eff},+}^2)\delta\chi_+ \\ + (D_0 + D_1\chi_{\text{eff},+} + D_2\chi_{\text{eff},+}^2 + D_3\chi_{\text{eff},+}^3) = 0, \end{aligned} \quad (5.7)$$

$$\begin{aligned} \delta\mu\delta\chi_-^3 + (B_0 + B_1\chi_{\text{eff},-})\delta\chi_-^2 \\ + (C_0 + C_1\chi_{\text{eff},-} + C_2\chi_{\text{eff},-}^2)\delta\chi_- \\ + (D_0 + D_1\chi_{\text{eff},-} + D_2\chi_{\text{eff},-}^2 + D_3\chi_{\text{eff},-}^3) = 0. \end{aligned} \quad (5.8)$$

Using the implicit function theorem we can get two equations, one satisfied by the positive roots $\delta\chi_+$ and $\chi_{\text{eff},+}$ [the derivative of Eq. (5.7)], and one satisfied by the negative roots $\delta\chi_-$ and $\chi_{\text{eff},-}$ [the derivative of Eq. (5.8)]:

$$\begin{aligned} B'_0\delta\chi_+^2 + (C'_0 + C'_1\chi_{\text{eff},+})\delta\chi_+ + (D'_0 + D'_1\chi_{\text{eff},+} + D'_2\chi_{\text{eff},+}) \\ + (3\delta\mu\delta\chi_+^2 + 2B\delta\chi_+ + C\delta\chi_+)\delta\chi'_+ \\ + (B_1\chi_{\text{eff},+}\delta\chi_+^2 + (C_1 + 2C_2\chi_{\text{eff},+})\delta\chi_+ \\ + (D_1 + 2D_2\chi_{\text{eff},+} + 3D_3\chi_{\text{eff},+}^2))\chi'_{\text{eff},+} = 0, \end{aligned} \quad (5.9)$$

$$\begin{aligned} B'_0\delta\chi_-^2 + (C'_0 + C'_1\chi_{\text{eff},-})\delta\chi_- + (D'_0 + D'_1\chi_{\text{eff},-} + D'_2\chi_{\text{eff},-}) \\ + (3\delta\mu\delta\chi_-^2 + 2B\delta\chi_- + C\delta\chi_-)\delta\chi'_- \\ + (B_1\chi_{\text{eff},-}\delta\chi_-^2 + (C_1 + 2C_2\chi_{\text{eff},-})\delta\chi_- \\ + (D_1 + 2D_2\chi_{\text{eff},-} + 3D_3\chi_{\text{eff},-}^2))\chi'_{\text{eff},-} = 0, \end{aligned} \quad (5.10)$$

where the primes denote time derivatives. These can be obtained using the definitions of the coefficients, B , C , and D in conjunction with the time derivatives of J and y ; as an example B'_0 is given as

$$B'_0 = \frac{\partial B_0}{\partial J} \frac{d\langle J \rangle}{dt} + \frac{\partial B_0}{\partial y} \frac{dy}{dt}. \quad (5.11)$$

A second set of relations follows from the derivatives directly, giving a complete set of equations:

$$\chi'_{\text{eff},+} = \frac{yA_{\chi_{\text{eff},\delta\chi}}\delta\chi_+ + yA_{\chi_{\text{eff},\chi_{\text{eff},+}}}\chi_{\text{eff},+}}{1 + yA_{\delta\chi,\delta\chi}\delta\chi_+ + yA_{\delta\chi,\chi_{\text{eff},+}}\chi_{\text{eff},+}} \delta\chi'_+, \quad (5.12)$$

$$\chi'_{\text{eff},-} = \frac{yA_{\chi_{\text{eff}},\delta\chi}\delta\chi_- + yA_{\chi_{\text{eff}},\chi_{\text{eff}}}\chi_{\text{eff},-}}{1 + yA_{\delta\chi,\delta\chi}\delta\chi_- + yA_{\delta\chi,\chi_{\text{eff}}}\chi_{\text{eff},-}} \delta\chi'_-. \quad (5.13)$$

The derivative of the averages is then straightforwardly obtained from the solutions to these via

$$\frac{d\langle\delta\chi\rangle}{dt} = \frac{1}{2}(\delta\chi'_+ + \delta\chi'_-) \quad (5.14a)$$

$$\frac{d\langle\chi_{\text{eff}}\rangle}{dt} = \frac{1}{2}(\chi'_{\text{eff},+} + \chi'_{\text{eff},-}). \quad (5.14b)$$

In the absence of radiation reaction the derivatives of y and J are zero, and consequently the derivatives of the coefficients (B'_0 , B'_1 , C'_0 , etc.) are zero. The solution to the resulting system of equations is $\delta\chi'_+ = \delta\chi'_- = \chi'_{\text{eff},+} = \chi'_{\text{eff},-} = 0$. This proves that in the absence of radiation reaction the averages do not evolve.

C. Summarizing

At this point, we have discussed all the equations necessary for describing the spin dynamics under the influence of radiation reaction. Our method is summarized

in Fig. 1 in the form of a flow chart. The general idea can be broken up into several blocks, which can be described generally as initializing the averages (red), updating the averages (yellow), and calculating the periodic part (green). The first two deal with the secular parts, while the latter is critical for accounting for the effects of precession. Once the evolution of these key quantities is known, the waveform is generated using standard techniques (see, e.g., [[22], Sec. IV]). Following [21], we refer to the resulting waveform as a frequency domain waveform because, while the equations are evolved in the time domain, these time domain solutions can be transformed directly to frequency domain waveforms via the method of shifted uniform asymptotics (as opposed to constructing a time domain waveform and then transforming this to the frequency domain). We do not present the equations to produce this waveform here because they are identical to those found in [[22], Sec. IV]. In the analysis here, we only use the leading term in $dy/dt = (32\eta/5)y^9$ unless otherwise specified. When constructing realistic waveforms for actual analysis of gravitational waves, this should be updated with the most current PN expression for dy/dt . Thus, to include the effects of higher PN results for the nonspinning part one should adjust dy/dt as well as modify the expressions for the nonspinning part appearing in the waveform generation.

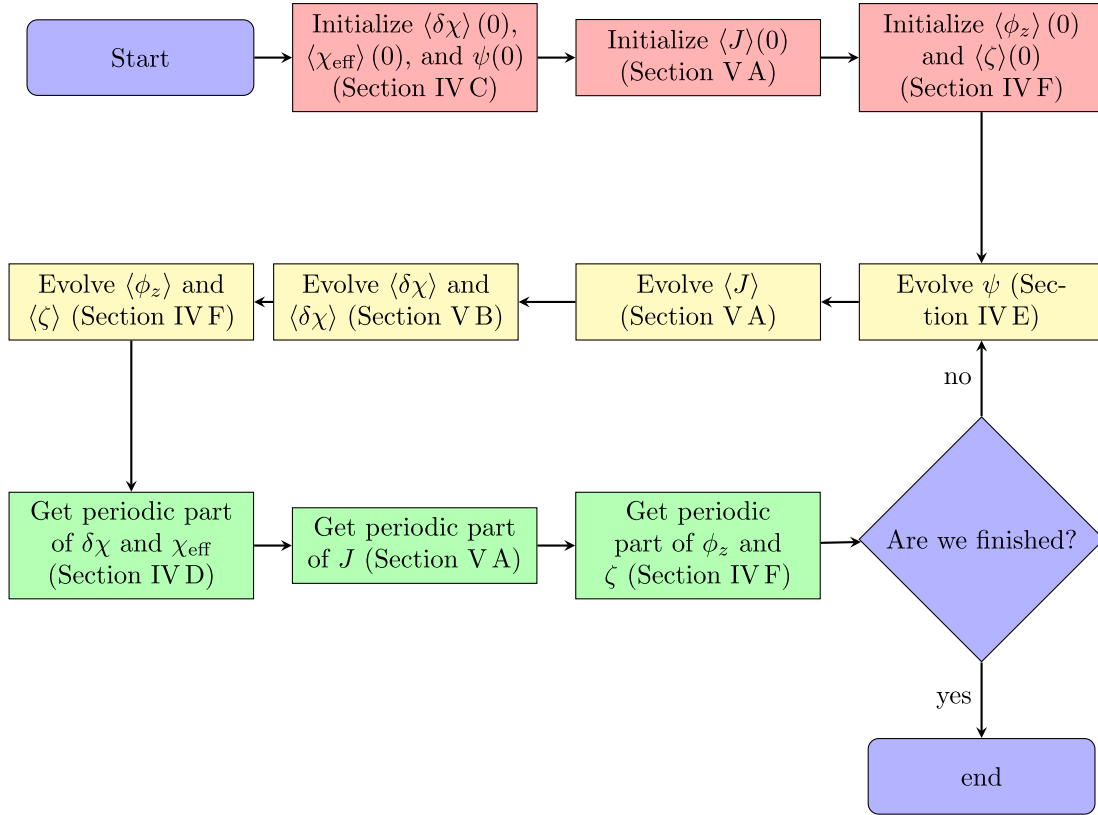


FIG. 1. This flow chart summarizes the key steps in solving for the precession equations of compact objects (with possibly $\kappa \neq 1$) on circular orbits. The parts in red initialize the averages, the parts in yellow update the averages, and the parts in green evolve the periodic parts of the solutions.

VI. COMPARING MODELS

In this section, we first establish the validity of our method in Sec. VIA before we compare waveforms of various binaries in Sec. VIB. In Sec. VIA we compute the difference between the waveform constructed according to the discussion in Secs. IV and V and the waveform following numerical evolution of spins. The latter section describes the key results of this paper: It shows that the quadrupole κ_i has an observable imprint on the waveform, at least for some of the spin/orbital configurations.

A. Model validation

To evaluate the effectiveness of the proposed method, we compare the method to the fully numerically evolved precession equation Eq. (2.8). Our method is better than simply numerically evolving the precession equations directly because of the timescales on which they can be accurately evolved (while still accounting for the full effects of precession). To numerically evolve the precession equations one must evolve them on the precession timescale; otherwise they run the risk of diverging. These divergences usually occur as a result of one point lying outside the upper or lower bound on $\delta\chi$ or χ_{eff} ; the solution then diverges secularly. To avoid this behavior, one typically has to use an overly expensive number of points in the evolution to keep the error low. Our solution has no such issues. Since we are evolving the average values, there is no chance of such an issue happening in the first place, and it can be accurately evolved on the radiation reaction timescale. Because of the different timescales on which the system must be evolved, our method takes on average 5.1 ms evolving from 10 to 100 Hz with a single CPU for the system configurations in this section, while evolving the precession equations numerically (while keeping enough points to avoid the aforementioned divergence) takes on average 54 ms evolving from 10 to 100 Hz with a single CPU for the same configurations. For high SNR events with better detector sensitivity, the waveform will be longer so this speed-up factor will be larger. Our method is only constrained by how many frequency points one wants to evaluate, while the full numerical evolution is constrained by the precession timescale.

As concrete examples for comparison, we examine two systems: a binary comprised of two neutron stars and a binary consisting of one neutron star and one black hole. For these comparisons we will use $\chi_1 = 0.4$ and $\chi_2 = 0.7$ for the spins; we set the angles of \vec{s}_1 and \vec{s}_2 relative to \hat{L} as $\theta_{s1} = \pi/20$, $\phi_{s1} = 0$, $\theta_{s2} = \pi/4$, $\phi_{s2} = \pi/10$. The only differences between the NSNS and NSBH systems we analyze are the masses and spin-induced quadrupole moment constants:

- (i) For NSNS binaries, we will use $M_1 = 2.6M_\odot$, $M_2 = 1.5M_\odot$, $\kappa_1 = 2.5$, $\kappa_2 = 3.5$.

- (ii) For NSBH binaries, we will use $M_1 = 23.0M_\odot$, $M_2 = 2.6M_\odot$, $\kappa_1 = 1.0$ and $\kappa_2 = 2.5$.

Here we have chosen values of κ that are smaller than the typical range for neutron stars ($\kappa \sim 4\text{--}8$ [30]) to be conservative in examining whether this is potentially measurable. To facilitate the comparison, the tidal effects of NSs are not included here, although their implementation is straightforward to add.

We start by looking at several spin variables as a function of frequency to determine whether or not our method well approximates the spin dynamics. In Fig. 2 are plots of θ_L and ϕ_z (the spin variables most relevant to waveform generation) for the binary neutron-star (BNS) and NSBH systems described above.

From these we can see that there is a good agreement between the spin variables produced via our method and those computed numerically. The agreement between the precession frequencies is important, since small differences in the precession frequency affect the waveform more than small differences in the amplitude or average. The error between the numerical and our method is minimal at the extrema of the oscillations; this is a result of how we approximated the solution as the first term in their Fourier series (i.e., the “ $m = 0$ ” approximation), since we defined the amplitude and average in such a way that the extrema of $\delta\chi$ and χ_{eff} are their true values.

While looking at the spin variables is insightful to verify that our method reproduces the spin dynamics accurately, the most important check is how well the produced waveforms match. To examine this, we look at two sets of systems.

The first set involves evaluating the effectiveness for general NSNS systems (since they are more difficult than NSBH systems, so present a good test of accuracy); we evenly space the first mass between $1.8M_\odot$ and $2.6M_\odot$, and for the second we distribute its mass evenly between $1.0M_\odot$ and $0.9m_1$ (to ensure that the mass ratio is not equal to 1). We set the first spin to be $\chi_1 = 0.7$, and the second to be $\chi_2 = 0.2$; we then evenly distribute the angles θ_{s1} , θ_{s2} , and ϕ_{s2} every 20° over the sphere, evolving every system from 10 to 100 Hz.

The second set of systems is more restricted in order to explore how much error is produced for models similar to GW190814, since this is the system of interest to us. In particular, we restrict the masses to $m_1 = 23M_\odot$ and $m_2 = 2.6M_\odot$, and the spins to $\chi_1 = \chi_2 = 0.6$. Similarly we distribute the angles θ_{s1} , θ_{s2} , and ϕ_{s2} every 20° over the sphere, evolving every system from 10 to 100 Hz.

We use the overlap, defined as

$$\mathcal{O}(h_1, h_2) = \frac{(h_1, h_2)}{\sqrt{(h_1, h_1)(h_2, h_2)}},$$

$$(h_1, h_2) = 4\text{Re} \int_{f_{\min}}^{f_{\max}} h_1(f)h_2^*(f)df, \quad (6.1)$$

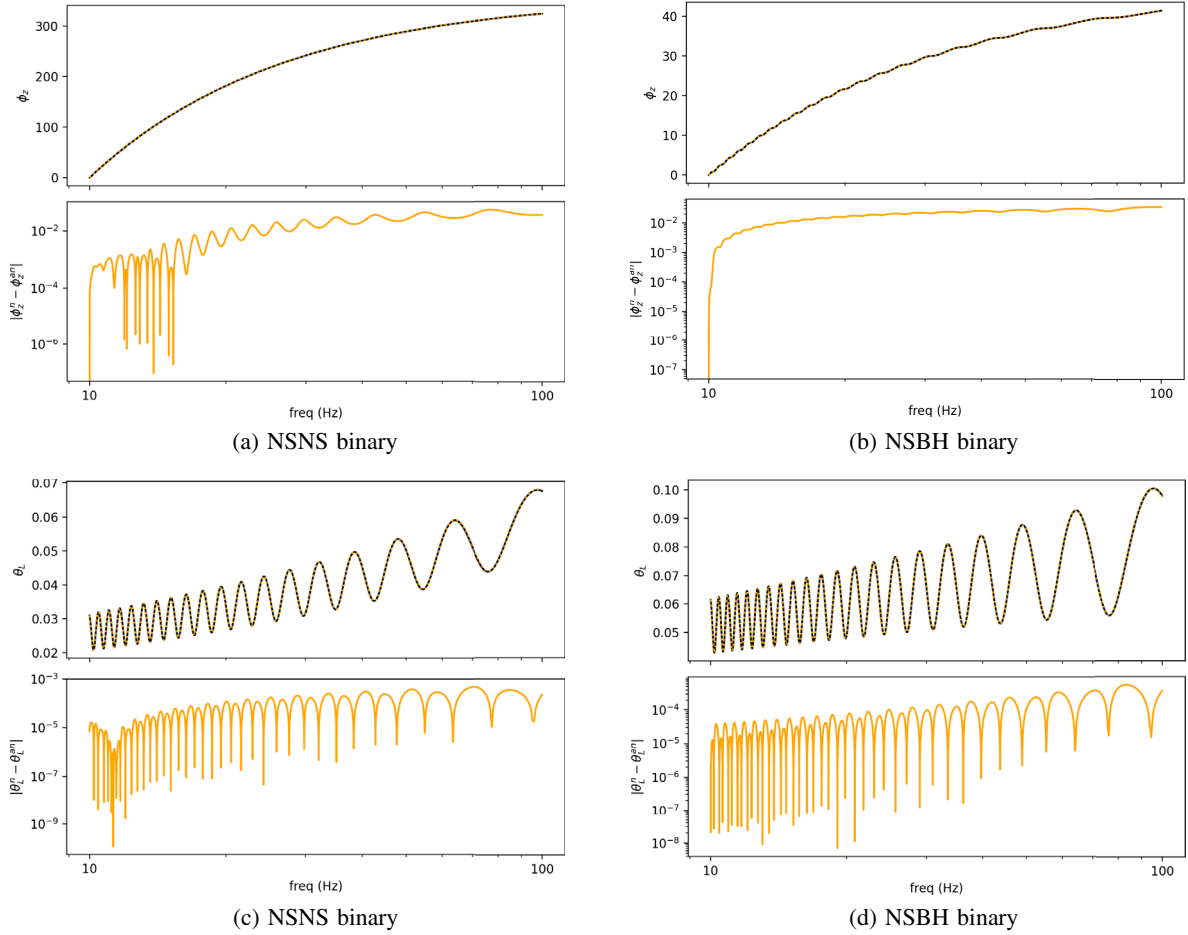


FIG. 2. Plot of ϕ_z vs frequency for the NSNS (NSBH) binary in panel (a) [(b)], and θ_L for the NSNS (NSBH) binary in panel (c) [(d)]. In each plot the black curve is the numerically evolved system, while the orange curves are the solution found using the method outlined in this paper. The top panels show the actual values of ϕ_z/θ_L , while the bottom panels show the absolute error of the quantity produced with our method vs the numerically evolved one.

where the waveform phase is aligned at the initial frequency. We do not minimize the coalescence phase and time here; this is to produce a more conservative estimate of the accuracy of the waveform since the waveform should be accurate assuming they start with the same initial phase with or without minimization. The cumulative distribution functions (CDFs) of one minus the overlap between the waveform produced via our method and the waveform produced via the full numerical evolution are shown in Fig. 3.

For the set of binary neutron star systems we examined, we find that only 1.35%(7.44%) have an overlap worse than 0.965(0.994). This is the same order of magnitude as in [21]. We have investigated several of the cases with larger values of $1 - \mathcal{O}$, and find that the main reason for these larger values is the noninclusion of higher terms in the Fourier series of our “ $m = 0$ ” approximation. This is because in these cases, θ_L drifts close to zero at its minimum. A small error in the value of θ_L at this point then introduces larger effects in the secular evolution of ϕ_z . When the system precesses away from θ_L being close to zero, this then poses an issue and in turn contributes to the

larger value of $1 - \mathcal{O}$. Adding more terms in the approximation would make this error smaller, in principal allowing us to reduce $1 - \mathcal{O}$. In the NSBH case no systems we examined have overlap worse than 0.999.

B. Differences between BNS/NSBH and BBH Waveforms

Having established the excellent accuracy of our method with mismatch less than 3.5% for 98.65% in the more extreme case of NSNS systems (and an order of magnitude better accuracy in black-hole neutron-star (BHNS) systems), here we study the qualitative effects of the spin-induced quadrupole moment on the evolution. In order to do so, we compare the two systems in Sec. VI A to BHBH with the same parameters, except with $\kappa_1 = 1 = \kappa_2$.

Here we follow a similar procedure as in the previous section, using the same two sample configurations to evolve the NSNS/NSBH systems and then evolve the same system as though they were a BHBH system (with the other parameters all the same).

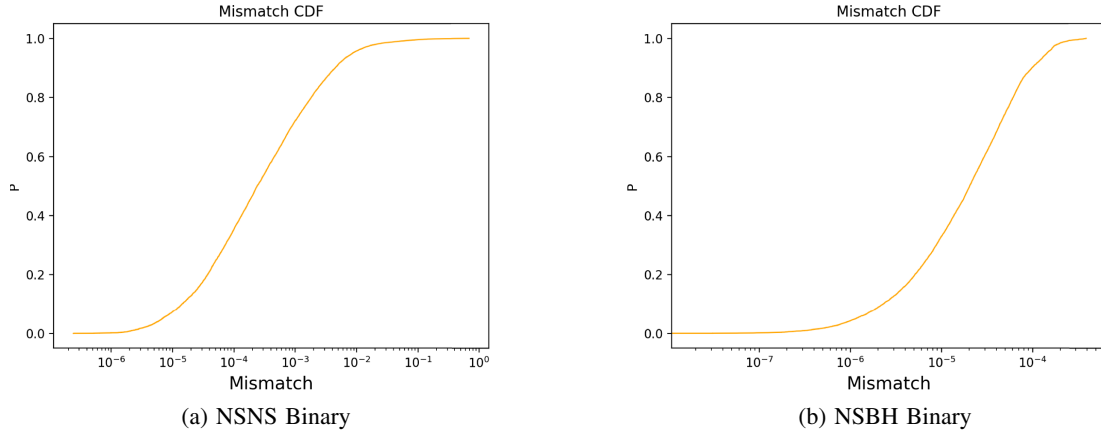


FIG. 3. Plots of the CDF for $1 - \mathcal{O}$ between the numerically evolved NSNS/NSBH systems and the same systems evolved with our method.

First, the effect of the quadrupole moment on θ_L and ϕ_z is shown in Fig. 4 to determine qualitatively what effect the spin-induced quadrupole constant has on the spin dynamics. Looking at the angle ϕ_z in Fig. 4, the difference

between the NSNS and BHBH case is large enough that it is directly visible, and the difference accumulates to several radians. The source of this secular effect is the corrections to the terms in the derivative of the average, Eq. (4.29),

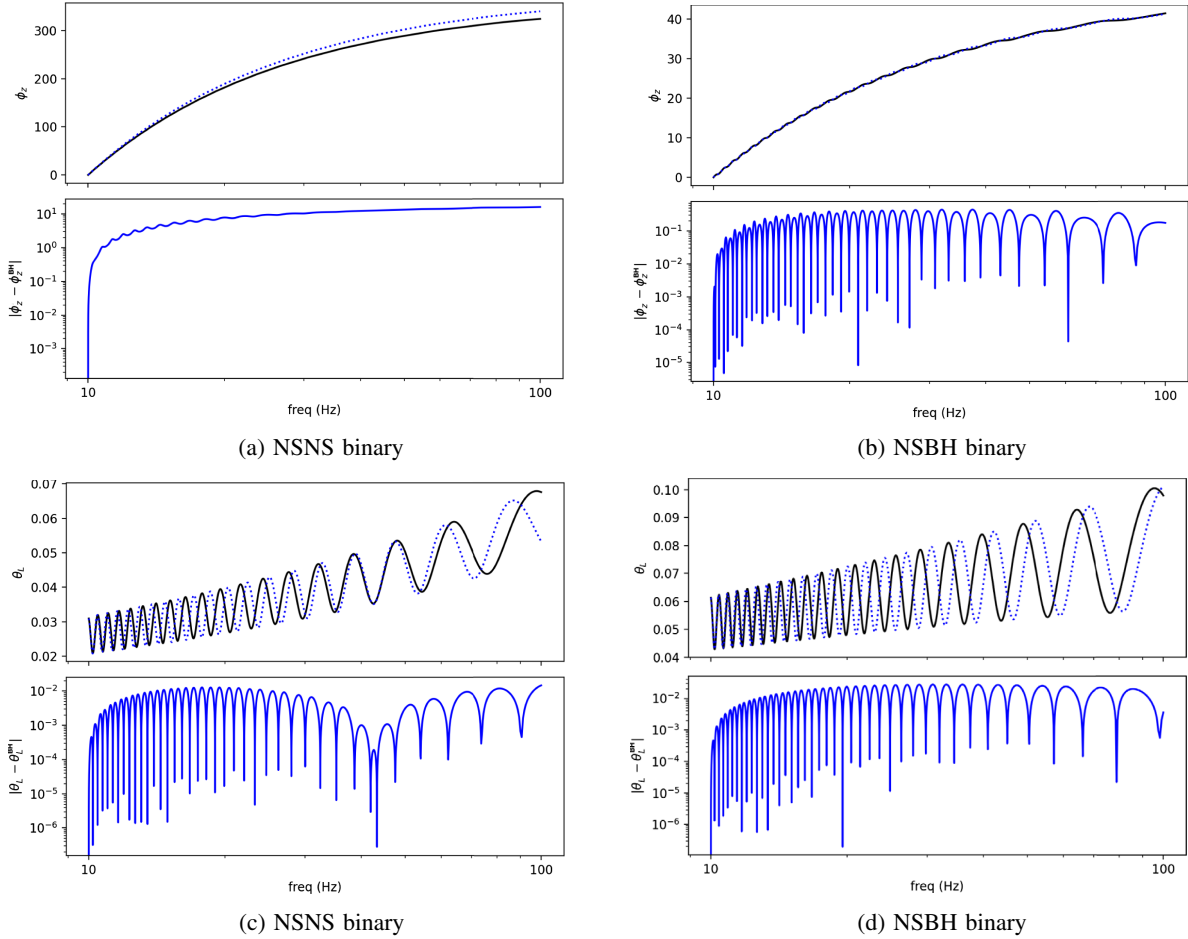


FIG. 4. Plot of ϕ_z vs frequency for the NSNS (NSBH) binary in panel (a) [(b)], and θ_L for the NSNS (NSBH) binary in panel (c) [(d)]. In each plot the black curve is the numerically evolved neutron star system, while the blue curves are the corresponding BBH systems. The top panels show the actual values of ϕ_z/θ_L , while the bottom panels show the absolute difference between the NSNS/NSBH and BHBH binaries.

involving $Q_{11} - Q_{16}$. Thus, the effects of the spin-induced quadrupole moment are important and introduce potentially large errors to the waveform if left unaccounted for, even for smaller quadrupole moment constants between 1.1 and 1.5. This increase in the rate of change of ϕ_z corresponds to a change to the precession frequency due to the change in the spin-induced quadrupole moment; this is also observed in θ_L as an increase in the rate at which the oscillations occur.

The difference between the NSBH and BHBH systems is not secular but periodic in nature, characterized by the sharp, repeating dips. This is because the secular part for a NSBH system is suppressed by the mass ratio. Intuitively, this makes sense: the larger body's spin-induced quadrupole moment affects the waveform more. In the NSNS case, both masses are similar, whereas the masses can differ significantly in a NSBH binary. For the NSBH case we considered, the mass ratio is large so the secular part of the evolution of ϕ_z is little affected by the quadrupole moment of the light neutron star. In both cases in θ_L we observe little secular deviation; it is largely periodic.

To accurately assess the measurability of these effects we will use the mismatch, defined as

$$\mathcal{M} = 1 - \max_{\phi_c, t_c} \frac{(h_1, h_2)}{\sqrt{(h_1, h_1)(h_2, h_2)}},$$

$$(h_1, h_2) = 4\text{Re} \int_{f_{\min}}^{f_{\max}} \frac{h_1(f)h_2^*(f)}{S_n(f)} df, \quad (6.2)$$

where now we perform matched filtering, maximizing the overlap integral over the initial phase and time (or equivalently minimizing the mismatch), and we also include the advanced LIGO zero-detuned, high power noise sensitivity [31]. So that we can accurately determine the magnitude of these effects with everything accounted for, we include the higher order terms in dy/dt and the contributions of the quadrupole moment constant to the nonspinning part of the waveform [7]. The CDF of the mismatch between the BHNS/BNS waveform and the corresponding BBH waveform is shown in Fig. 5. We fix the masses and quadrupole moment constants to those indicated in each panel in the figure; the dimensionless spins are fixed to $\chi_1 = 0.7$ and $\chi_2 = 0.6$ for the upper two panels and to illustrate a more conservative case $\chi_1 = 0.3$ and $\chi_2 = 0.2$ for the lower two panels. Qualitatively the distributions are similar for the more conservative spin cases, but with an order of

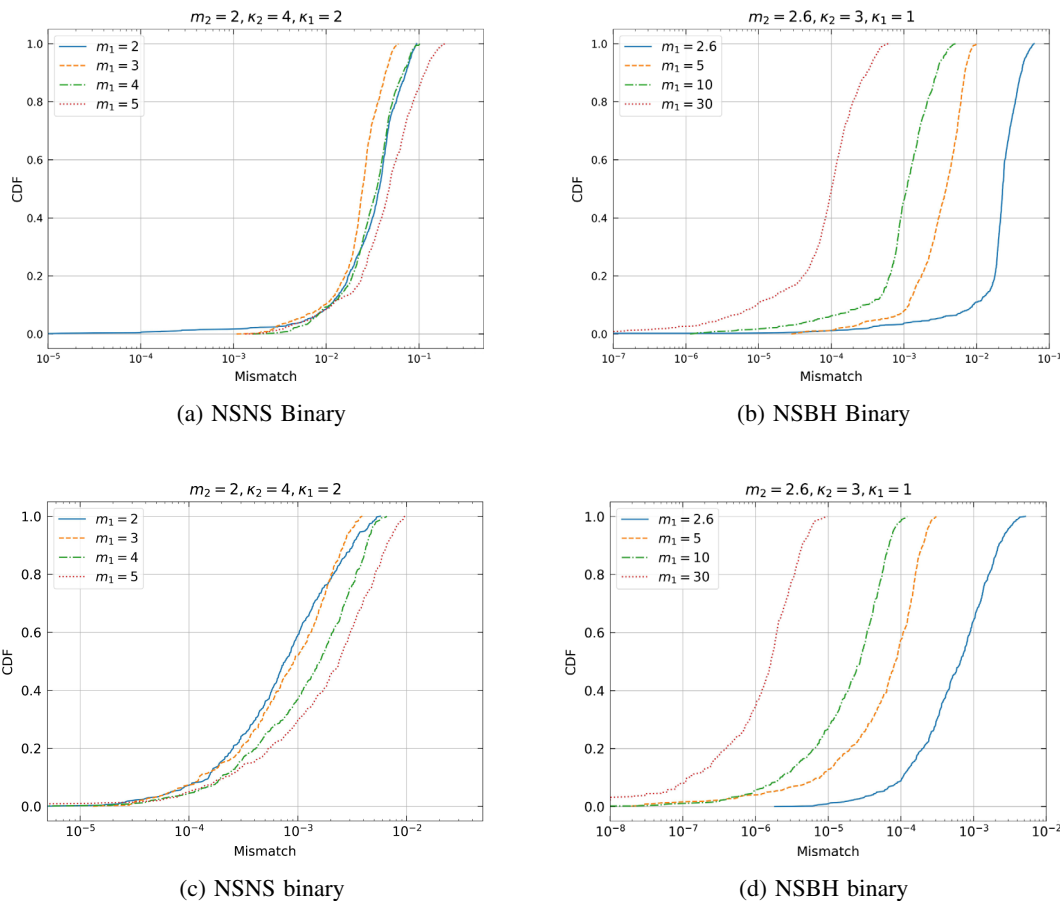


FIG. 5. Plots of the CDF for mismatch between the numerically evolved NSNS/NSBH systems and the corresponding numerically evolved BHBH system.

magnitude smaller mismatch. We take 1000 samples with these inputs with randomly distributed isotropic spin angles and inclination angle.

For the neutron star binary, this effect produces a large mismatch; however for the NSBH system this effect is more difficult to measure. The explanation is that the secular effect (which is easier to measure than periodic deviations) is suppressed by the mass ratio, which is small in the higher mass ratio BHNS cases we examine. We can see this directly in the second panel of Fig. 5, where the average mismatch between the NSBH system and the corresponding BBH system decreases with increasing mass ratio.

By examining which cases have the lowest mismatch, we find that the effects on the spin precession are minimized for spins that lie in the plane perpendicular to the orbital angular momentum. This can be understood intuitively from the precession equations [Eq. (2.8)]; while the precession is larger for spins perpendicular to the orbital angular momentum, this is not the hypothetical best place to find the *difference* in the precession. This is because the correction terms scale with the projection of the spin onto the orbital angular momentum, so the difference is at a minimum when they are perpendicular.

The mismatch is nonzero here for spin aligned cases due to the contributions to the nonprecessing waveform from the quadrupole moment, but these constitute cases below the median mismatch, indicating that the effects on the precession dominate the waveform over the effects on the nonprecessing part when the system is precessing (when the spins are not aligned with the orbital angular momentum). As noted in [7], in the aligned spin case, the effects on the waveform due to the quadrupole moment are larger than those of the tidal deformability. The main issue is that the effects on the nonprecessing part of the waveform are degenerate with changes to the component masses and spins, which is confirmed in the parameter estimation in [32] for potential black hole mimickers. Even for the spin-aligned case, Harry and Hinderer note that neglecting the quadrupole moment contributions will lead to biases, so its inclusion is still important. This is compounded by the facts that the precessional effects cause larger mismatch and are more difficult to mimic with changes to the component masses and spins, making them easier to measure than the nonprecessing effects and potentially breaking the degeneracy.

The effects of the spin-induced quadrupole constant have likewise been examined for aligned-spin cases elsewhere [33–35]. In agreement with these results, we find that the effects are more noticeable when the first spin is larger, because the secondary’s spin affects the waveform less. As they note, for the dimensionless spin magnitudes used here, constraints on the order of $O(1)$ can be placed on the spin-induced quadrupole constant with second-generation detectors. Since the precession introduces larger mismatch than the nonprecession part, precession only

improves our ability to measure the difference. For a mass-gap object, this can potentially allow the objects to be distinguished from black holes.

The tidal heating effect, which comes from the energy and angular momentum on the black hole horizon, contributes at 2.5 PN order to the waveform if the black hole is spinning [36], and 4 PN if the black hole is nonspinning [37]. Since neutron stars do not have tidal heating effects, in principle the tidal heating effect can also be used to probe the nature of mass-gap objects. However, the calculation in [38] shows that the tidal heating effect from an equal mass black hole (with high spin $a = 0.998$) binary contributes to ~ 0.05 gravitational wave cycle, which is approximately 0.3 rad in phase modulation. For unequal mass ratio binaries, the flux absorbed by the less massive black hole M_2 is roughly M_2/M_1 times smaller than the flux absorbed by M_1 , if both black holes are spinning, and $(M_2/M_1)^2$, if both are nonspinning. As a result, replacing M_2 by a neutron star in a GW 190814-like binary has negligible impact on the gravitational wave phase if only the tidal heating effect is considered.

VII. CONCLUSION

We have presented a new method to construct frequency domain waveforms for circular compact object binaries that include neutron stars. Because of the analytical treatment of the spin evolution equations, the spin variables are evolved on the radiation reaction timescale, which is convenient to transform to the frequency domain. The new waveform is able to achieve more than an order of magnitude speed-up compared with the one with fully numerical evolution of spins on the precession timescale. For generic mass ratio and spin configurations, one minus the overlap between the new waveform and the one with a fully numerical evolution of spins is $\leq 3.5\%$ for 98.65% of the configurations examined. We have also investigated the difference between BHBH, NSNS, and NSBH waveforms due to different spin-induced quadrupole moment constant values, assuming the same component mass and spins and neglecting possible tidal effects. We find that the maximum difference occurs for systems with somewhat aligned or antialigned spins. In such cases the mismatch between BHBH and BNS waveforms can be approximately $\sim 10\%$, which is promising for detection with Advanced LIGO/Virgo [31,39] and LIGO A+ [40]. For other spin configurations, the differences between the waveforms are rather small, which may require third-generation gravitational wave detectors to measure the spin-induced quadrupole moment constant. For BNS systems, if the neutron stars have significant spins, the mismatch may reach 5% for a good fraction of spin configurations. This is particularly interesting if in the future we discover BNS systems with two mass-gap objects.

There are several avenues for further developments, such as, first, improving this waveform’s speed and accuracy via

a semianalytic evolution. This can be done by expanding the averages and amplitudes of $\delta\chi$ and χ_{eff} in a series in terms of the PN parameter y :

$$\begin{aligned}\langle\chi\rangle &= \langle\delta\chi\rangle_0 + \langle\delta\chi\rangle_1 y + \langle\delta\chi\rangle_2 y^2, \\ G_{\delta\chi} &= G_{\delta\chi,0} + G_{\delta\chi,1} y + G_{\delta\chi,2} y^2, \\ \langle\chi_{\text{eff}}\rangle &= \langle\chi_{\text{eff}}\rangle_0 + \langle\chi_{\text{eff}}\rangle_1 y + \langle\chi_{\text{eff}}\rangle_2 y^2, \\ G_{\chi_{\text{eff}}} &= G_{\chi_{\text{eff}},0} + G_{\chi_{\text{eff}},1} y + G_{\chi_{\text{eff}},2} y^2.\end{aligned}\quad (7.1)$$

This approach has the advantage that while there is a higher upfront cost to initialize this system (requiring solving a system of linear equations), it makes the cost of calculating the amplitudes and averages at each step significantly lower and removes the need for root finding altogether. The system of equations for these coefficients would be formed from the initial values of the amplitudes and averages, which can be found using a similar set of derivatives of $\delta\chi$ and χ_{eff} used to calculate the initial averages here. The rest of the equations would be formed from derivatives of the roots of $\delta\chi$ and χ_{eff} ; we have discussed in an earlier section how to find such derivatives via the implicit function theorem. To keep high accuracy in the waveform, ψ and $\langle\phi_z\rangle$ could potentially still be numerically evolved if necessary.

Normally speed versus accuracy is a balancing act: Improving one typically harms the other. The approach taken in this paper provides the potential for improving both simultaneously. The speed improvement we mentioned already and the accuracy can be further improved by including the next terms in the Fourier series in the “ $m = 0$ ” approximation. The higher order terms improve the accuracy in two ways. First, including them makes the estimation of the average and amplitude of $\delta\chi$ and χ_{eff} more accurate, thereby lowering the periodic effects in the error plots of θ_L which correspond to $1\times$ the precession frequency. On top of this, the inclusion of the higher order terms should remove additional error that is not currently dominant visually with double the frequency. This improvement in θ_L will also improve the accuracy of ϕ_z 's evolution, since the main source of error in ϕ_z is due to the error in the minimum of θ_L .

Currently, there is no waveform model that can simultaneously handle the evolution of eccentric orbits and precession. For neutron star binaries this task is particularly complicated as tidal excitations may include multiple harmonics with eccentric orbits [41,42]. However, this is (astro)physically important as some of the dynamically formed binaries may carry nonzero eccentricity and non-negligible precession at the same time. It is a promising direction to consider whether eccentric orbit evolution can be incorporated into the scheme discussed here.

Finally, it will be interesting to perform Bayesian parameter estimation with this waveform, either with the real data (such as GW 190814) or with artificial data

(detector noise plus injected signal). Given that this is probably the best method to probe the nature of the mass-gap objects similar to the one found in GW 190814—if no electromagnetic counterparts are present—it is important to assess the ability of using these precession waveforms to measure the spin-induced quadrupole moment constant in compact binaries with respect to various detector sensitivities. We are currently performing such analysis; the results will be reported in a future publication.

ACKNOWLEDGMENTS

We thank Mohammed Khalili for reading over the manuscript and providing many helpful comments. We thank Reed Essick and the Perimeter LSC discussion group for useful discussions. M. L., Z. L., and H. Y. are supported by the Natural Sciences and Engineering Research Council of Canada and in part by Perimeter Institute for Theoretical Physics. Research at Perimeter Institute is supported in part by the Government of Canada through the Department of Innovation, Science and Economic Development Canada and by the Province of Ontario through the Ministry of Colleges and Universities. This work was supported by the National Natural Science Foundation of China (11975027).

APPENDIX A: COEFFICIENTS OF $d\delta\chi/dt$ WITH BEHAVIOR SEPARATED

The coefficients in Eqs. (3.1) and (3.2) can be found in Klein [22], but are repeated here:

$$\begin{aligned}B &= \frac{y}{2\eta^2} [-2\eta(J^2 - L^2 - L\chi_{\text{eff}}) + \delta\mu(S_1^2 - S_2^2) \\ &\quad - \delta\mu^2(2L^2 + S_1^2 + S_2^2)],\end{aligned}\quad (A1a)$$

$$\begin{aligned}C &= \frac{y}{2\eta^2} \{ (1 + \delta\mu^2)\chi_{\text{eff}}(S_1^2 - S_2^2) \\ &\quad + 2\delta\mu[2L(J^2 - L^2 - L\chi_{\text{eff}}) \\ &\quad - (2L + \chi_{\text{eff}})(S_1^2 + S_2^2) - \eta L\chi_{\text{eff}}^2] \}\end{aligned}\quad (A1b)$$

$$\begin{aligned}D &= \frac{y}{2\eta^2} \{ -2(J^2 - L^2 - L\chi_{\text{eff}})[J^2 - L^2 \\ &\quad - L\chi_{\text{eff}} - 2(S_1^2 + S_2^2) - \eta\chi_{\text{eff}}^2] \\ &\quad + (S_1^2 - S_2^2)[\delta\mu\chi_{\text{eff}}^2 - 2(S_1^2 - S_2^2)] \\ &\quad - \chi_{\text{eff}}^2(S_1^2 + S_2^2) \}.\end{aligned}\quad (A1c)$$

From these it follows that the coefficients with the behavior of χ_{eff} separated [see Eq. (4.21)] are

$$\begin{aligned}B_0 &= \frac{y}{2\eta^2} [-2\eta(J^2 - L^2) + \delta\mu(S_1^2 - S_2^2) \\ &\quad - \delta\mu^2(2L^2 + S_1^2 + S_2^2)]\end{aligned}\quad (A2a)$$

$$B_1 = 1\quad (A2b)$$

$$C_0 = \frac{2\delta\mu}{\eta} [J^2 - L^2 - S_1^2 - S_2^2] \quad (\text{A3a})$$

$$C_1 = \frac{y}{2\eta^2} [(1 + \delta\mu^2)(S_1^2 - S_2^2) - 2\delta\mu(2L^2 + S_1^2 + S_2^2)] \quad (\text{A3b})$$

$$C_2 = -\delta\mu \quad (\text{A3c})$$

$$D_0 = \frac{-y}{\eta^2} (J^2 - L^2 - S_1^2 - 2S_1S_2 - S_2^2) \times (J^2 - L^2 - S_1^2 + 2S_1S_2 - S_2^2) \quad (\text{A4a})$$

$$D_1 = \frac{2}{\eta} (J^2 - L^2 - S_1^2 - S_2^2) \quad (\text{A4b})$$

$$D_2 = \frac{y}{2\eta^2} [2\eta(J^2 - L^2) - (2L^2 + S_1^2 + S_2^2) + \delta\mu(S_1^2 - S_2^2)] \quad (\text{A4c})$$

$$D_3 = -1. \quad (\text{A4d})$$

APPENDIX B: DERIVATIVE OF ϕ_z DEFINITIONS

We restate the derivative of ϕ_z here:

$$\frac{d\phi_z}{dt} = \frac{1}{\sin^2(\theta_L)} \left[\frac{d\hat{L}}{dt} \cdot (\hat{J} \times \hat{L}) \right]. \quad (\text{B1})$$

By substituting the derivative $d\hat{L}/dt$, we can separate the behavior into the terms that come from the quadrupole moment constant being $\neq 1$ and those that correspond to the black hole portion; doing so gives

$$\begin{aligned} \frac{d\phi_z}{dt} = & -\frac{y^6}{2\sin^2(\theta_L)} [\hat{L} \times (\mu_1\vec{s}_1 + \mu_2\vec{s}_2)] \cdot (\hat{J} \times \hat{L}) \\ & - \frac{3y^6}{2\sin^2(\theta_L)} [1 - y\chi_{\text{eff}}] \{ \hat{L} \times \vec{s}_1 + \hat{L} \times \vec{s}_2 \} \cdot (\hat{J} \times \hat{L}) \\ & + \frac{3y^7}{2\sin^2(\theta_L)} \{ (\kappa_1 - 1)(\hat{L} \cdot \vec{s}_1)(\hat{L} \times \vec{s}_1) \\ & + (\kappa_2 - 1)(\hat{L} \cdot \vec{s}_2)(\hat{L} \times \vec{s}_2) \} \cdot (\hat{J} \times \hat{L}). \end{aligned} \quad (\text{B2})$$

By relying on the definition of \vec{J} given in Eq. (2.7), in addition to the definition of θ_L as the angle between \vec{L} and \vec{J} the first term can be simplified substantially:

$$\begin{aligned} \frac{d\phi_z}{dt} = & \frac{Jy^6}{2} - \frac{3y^6}{2\sin^2(\theta_L)} [1 - y\chi_{\text{eff}}] \{ \hat{L} \times \vec{s}_1 + \hat{L} \times \vec{s}_2 \} \cdot (\hat{J} \times \hat{L}) \\ & + \frac{3y^7}{2\sin^2(\theta_L)} \{ (\kappa_1 - 1)(\hat{L} \cdot \vec{s}_1)(\hat{L} \times \vec{s}_1) \\ & + (\kappa_2 - 1)(\hat{L} \cdot \vec{s}_2)(\hat{L} \times \vec{s}_2) \} \cdot (\hat{J} \times \hat{L}). \end{aligned} \quad (\text{B3})$$

The latter terms correspond to neutron stars, while the former terms (alone) compose the entirety of the black hole case. To simplify the derivative of ϕ_z we start by looking at its expression in the black hole case. Substituting Eq. (4.2) gives

$$\left[\frac{d\phi_z}{dt} \right]^{\text{BH}} \approx \frac{Jy^6}{2} \left\{ Q_1 + Q_2 \sin(\psi) + \frac{(Q_3 + Q_4 \sin(\psi))(Q_5 + Q_6 \sin(\psi) + Q_7 \sin^2(\psi))}{Q_8 Q_9 (1 - \frac{Q_{10}}{Q_8} \sin(\psi))(1 + \frac{Q_{10}}{Q_9} \sin(\psi))} \right\}, \quad (\text{B4})$$

where

$$Q_1 = 1 + \frac{3}{2\eta} (1 - y\langle\chi_{\text{eff}}\rangle) \quad (\text{B5a})$$

$$Q_2 = -\frac{3}{2\eta} yG_{\chi_{\text{eff}}} \quad (\text{B5b})$$

$$Q_3 = -\frac{3(1+q)}{2q} (1 - y\langle\chi_{\text{eff}}\rangle) = \frac{1 - Q_1}{1 + q} \quad (\text{B5c})$$

$$Q_4 = \frac{3(1+q)}{2q} yG_{\chi_{\text{eff}}} = \frac{-Q_2}{1 + q} \quad (\text{B5d})$$

$$Q_5 = 4(1 - q)(S_1^2 - S_2^2) - (1 + q)(\delta\mu\langle\delta\chi\rangle + \langle\chi_{\text{eff}}\rangle) \times (\delta\mu\langle\delta\chi\rangle + (1 - 4\eta)\langle\chi_{\text{eff}}\rangle) \quad (\text{B5e})$$

$$Q_6 = -(1 + q)[(\delta\mu\langle\delta\chi\rangle + \langle\chi_{\text{eff}}\rangle)(\delta\mu G_{\delta\chi} + (1 - 4\eta)G_{\chi_{\text{eff}}}) + (\delta\mu G_{\delta\chi} + G_{\chi_{\text{eff}}})(\delta\mu\langle\delta\chi\rangle + (1 - 4\eta)\langle\chi_{\text{eff}}\rangle)] \quad (\text{B5f})$$

$$Q_7 = -(1 + q)(\delta\mu G_{\delta\chi} + G_{\chi_{\text{eff}}})(\delta\mu G_{\delta\chi} + (1 - 4\eta)G_{\chi_{\text{eff}}}) \quad (\text{B5g})$$

$$Q_8 = 2\langle J \rangle - \delta\mu\langle\delta\chi\rangle - \langle\chi_{\text{eff}}\rangle - 2L \quad (\text{B5h})$$

$$Q_9 = 2\langle J \rangle + \delta\mu\langle\delta\chi\rangle + \langle\chi_{\text{eff}}\rangle + 2L = 4\langle J \rangle - Q_8 \quad (\text{B5i})$$

$$Q_{10} = \delta\mu G_{\delta\chi} + G_{\chi_{\text{eff}}}. \quad (\text{B5j})$$

The rest of the terms, corresponding to the spin-induced quadrupole moment of the neutron star are given by

$$\frac{d\phi_z}{dt} = \left[\frac{d\phi_z}{dt} \right]^{\text{BH}} + \frac{Jy^6}{2} \left\{ \frac{Q_{11} + Q_{12} \sin(\psi) + (Q_{13} + Q_{14} \sin(\psi))(Q_{15} + Q_{16} \sin(\psi) + Q_{17} \sin^2(\psi))}{Q_8 Q_9 (1 - \frac{Q_{10}}{Q_8} \sin(\psi)) (1 + \frac{Q_{10}}{Q_9} \sin(\psi))} \right\}, \quad (\text{B6})$$

where

$$Q_{11} = -3y \frac{J^2 - L^2}{L\eta} [(\kappa_2 - 1)\mu_1(\langle \chi_{\text{eff}} \rangle - \langle \delta\chi \rangle) + (\kappa_1 - 1)\mu_2(\langle \chi_{\text{eff}} \rangle + \langle \delta\chi \rangle)] \\ + 3y \frac{S_1^2 - S_2^2}{L\eta} [(\kappa_2 - 1)\mu_1(\langle \chi_{\text{eff}} \rangle - \langle \delta\chi \rangle) - (\kappa_1 - 1)\mu_2(\langle \chi_{\text{eff}} \rangle + \langle \delta\chi \rangle)] \quad (\text{B7a})$$

$$Q_{12} = -3y \frac{J^2 - L^2}{L\eta} [(\kappa_2 - 1)\mu_1(G_{\chi_{\text{eff}}} - G_{\delta\chi}) + (\kappa_1 - 1)\mu_2(G_{\chi_{\text{eff}}} + G_{\delta\chi})] \\ + 3y \frac{S_1^2 - S_2^2}{L\eta} [(\kappa_2 - 1)\mu_1(G_{\chi_{\text{eff}}} - G_{\delta\chi}) - (\kappa_1 - 1)\mu_2(G_{\chi_{\text{eff}}} + G_{\delta\chi})] \quad (\text{B7b})$$

$$Q_{13} = \frac{3}{2}(\delta\mu\langle \delta\chi \rangle + \langle \chi_{\text{eff}} \rangle) \quad (\text{B7c})$$

$$Q_{14} = \frac{3}{2}(\delta\mu G_{\delta\chi} + G_{\chi_{\text{eff}}}) \quad (\text{B7d})$$

$$Q_{15} = 4yA_{\chi_{\text{eff}},\delta\chi}\langle \delta\chi \rangle^2 + 2(4yA_{\chi_{\text{eff}},\chi_{\text{eff}}}\langle \chi_{\text{eff}} \rangle + \mu_2\kappa_1 - \mu_1\kappa_2 + \delta\mu)\langle \delta\chi \rangle \\ + 4yA_{\chi_{\text{eff}},\delta\chi}\langle \chi_{\text{eff}} \rangle^2 + 2(\mu_2\kappa_1 + \mu_1\kappa_2 - 1)\langle \chi_{\text{eff}} \rangle \quad (\text{B7e})$$

$$Q_{16} = 2G_{\delta\chi}(4y(A_{\chi_{\text{eff}},\chi_{\text{eff}}}\langle \chi_{\text{eff}} \rangle + A_{\chi_{\text{eff}},\delta\chi}\langle \delta\chi \rangle) - \mu_1\kappa_2 + \mu_2\kappa_1 + \delta\mu \\ + 2G_{\chi_{\text{eff}}}(4y(A_{\chi_{\text{eff}},\chi_{\text{eff}}}\langle \chi_{\text{eff}} \rangle + A_{\chi_{\text{eff}},\delta\chi}\langle \delta\chi \rangle) + \mu_1\kappa_2 + \mu_2\kappa_1 - 1) \quad (\text{B7f})$$

$$Q_{17} = 4y(A_{\chi_{\text{eff}},\delta\chi}(G_{\delta\chi}^2 + G_{\chi_{\text{eff}}}^2) + 2A_{\chi_{\text{eff}},\chi_{\text{eff}}}G_{\delta\chi}G_{\chi_{\text{eff}}}). \quad (\text{B7g})$$

Using these definitions the entire derivative can be rewritten as

$$\frac{d\phi_z}{dt} \approx \frac{Jy^6}{2} \left\{ Q_1 + Q_2 \sin(\psi) + \frac{H_0 + H_1 \sin(\psi) + H_2 \sin^2(\psi) + H_3 \sin^3(\psi)}{(1 + H_- \sin(\psi))(1 + H_+ \sin(\psi))} \right\}, \quad (\text{B8})$$

where

$$H_0 = \frac{Q_3 Q_5 + Q_{11} + Q_{13} Q_{15}}{Q_8 Q_9} \quad (\text{B9a})$$

$$H_1 = \frac{Q_3 Q_6 + Q_5 Q_4 + Q_{12} + Q_{13} Q_{16} + Q_{14} Q_{15}}{Q_8 Q_9} \quad (\text{B9b})$$

$$H_2 = \frac{Q_3 Q_7 + Q_4 Q_6 + Q_{13} Q_{17} + Q_{14} Q_{16}}{Q_8 Q_9} \quad (\text{B9c})$$

$$H_3 = \frac{Q_4 Q_7 + Q_{14} Q_{17}}{Q_8 Q_9} \quad (\text{B9d})$$

$$H_- = -\frac{Q_{10}}{Q_8} \quad (\text{B9e})$$

$$H_+ = \frac{Q_{10}}{Q_9}. \quad (\text{B9f})$$

The angles appearing in the solutions for ϕ_z and ζ are related to the above expressions in the following way:

$$\Phi_0 = \frac{Jy^6}{2} \left\{ Q_1 + \frac{H_2 H_+ H_- - H_3 H_- - H_3 H_+}{H_+^2 H_-^2} \right\} \quad (\text{B10a})$$

$$\Phi_s = \frac{Jy^6}{2} \left\{ Q_2 + \frac{H_3}{H_+ H_-} \right\} \quad (\text{B10b})$$

$$\Phi_+ = \frac{Jy^6}{2} \left\{ \frac{H_0 H_+^3 - H_1 H_+^2 + H_2 H_+ - H_3}{(H_+ - H_-) H_+^2 \sqrt{1 - H_+^2}} \right\} \quad (\text{B10c})$$

$$\Phi_- = -\frac{Jy^6}{2} \left\{ \frac{H_0 H_-^3 - H_1 H_-^2 + H_2 H_- - H_3}{(H_+ - H_-) H_-^2 \sqrt{1 - H_-^2}} \right\} \quad (\text{B10d})$$

$$\Theta_0 = \frac{2L + \delta\mu\langle \delta\chi \rangle + \langle \chi_{\text{eff}} \rangle}{2J} \quad (\text{B10e})$$

$$\Theta_s = \frac{\delta\mu G_{\delta\chi} + G_{\chi_{\text{eff}}}}{2J}. \quad (\text{B10f})$$

- [1] R. Abbott *et al.*, GWTC-3: Compact Binary Coalescences Observed by LIGO and Virgo during the Second Part of the Third Observing Run, [arXiv:2111.03606](#).
- [2] R. Abbott *et al.*, GWTC-2: Compact Binary Coalescences Observed by LIGO and Virgo during the First Half of the Third Observing Run, *Phys. Rev. X* **11**, 021053 (2021).
- [3] B. P. Abbott *et al.*, GWTC-1: A Gravitational-Wave Transient Catalog of Compact Binary Mergers Observed by LIGO and Virgo during the First and Second Observing Runs, *Phys. Rev. X* **9**, 031040 (2019).
- [4] Eanna E. Flanagan and Tanja Hinderer, Constraining neutron star tidal Love numbers with gravitational wave detectors, *Phys. Rev. D* **77**, 021502 (2008).
- [5] B. P. Abbott *et al.*, GW170817: Observation of Gravitational Waves from a Binary Neutron Star Inspiral, *Phys. Rev. Lett.* **119**, 161101 (2017).
- [6] David Radice, Albino Perego, Francesco Zappa, and Sebastiano Bernuzzi, GW170817: Joint constraint on the neutron star equation of state from multimessenger observations, *Astrophys. J. Lett.* **852**, L29 (2018).
- [7] Ian Harry and Tanja Hinderer, Observing and measuring the neutron-star equation-of-state in spinning binary neutron star systems, *Classical Quantum Gravity* **35**, 145010 (2018).
- [8] Gonçalo Castro, Leonardo Gualtieri, Andrea Maselli, and Paolo Pani, Impact and detectability of spin-tidal couplings in neutron star inspirals, *Phys. Rev. D* **106**, 024011 (2022).
- [9] Huan Yang, William E. East, and Luis Lehner, Can we distinguish low mass black holes in neutron star binaries?, *Astrophys. J.* **856**, 110 (2018); **870**, 139(E) (2019).
- [10] Zhen Pan, Zhenwei Lyu, and Huan Yang, Mass-gap extreme mass ratio inspirals, *Phys. Rev. D* **105**, 083005 (2022).
- [11] Zhen Pan, Zhenwei Lyu, and Huan Yang, Wet extreme mass ratio inspirals may be more common for spaceborne gravitational wave detection, *Phys. Rev. D* **104**, 063007 (2021).
- [12] Zhen Pan and Huan Yang, Formation rate of extreme mass ratio inspirals in active galactic nuclei, *Phys. Rev. D* **103**, 103018 (2021).
- [13] R. Abbott *et al.*, GW190814: Gravitational waves from the coalescence of a 23 solar mass black hole with a 2.6 solar mass compact object, *Astrophys. J. Lett.* **896**, L44 (2020).
- [14] Kyriakos Vattis, Isabelle S. Goldstein, and Savvas M. Koushiappas, Could the $2.6M_{\odot}$ object in GW190814 be a primordial black hole?, *Phys. Rev. D* **102**, 061301 (2020).
- [15] Daniel A. Godzieba, David Radice, and Sebastiano Bernuzzi, On the maximum mass of neutron stars and GW190814, *Astrophys. J.* **908**, 122 (2021).
- [16] Elias R. Most, L. Jens Papenfort, Lukas R. Weih, and Luciano Rezzolla, A lower bound on the maximum mass if the secondary in GW190814 was once a rapidly spinning neutron star, *Mon. Not. R. Astron. Soc.* **499**, L82 (2020).
- [17] Raissa F. P. Mendes and Huan Yang, Tidal deformability of boson stars and dark matter clumps, *Classical Quantum Gravity* **34**, 185001 (2017).
- [18] Vitor Cardoso and Paolo Pani, Testing the nature of dark compact objects: A status report, *Living Rev. Relativity* **22**, 4 (2019).
- [19] A. Nagar *et al.*, Time-domain effective-one-body gravitational waveforms for coalescing compact binaries with nonprecessing spins, tides and self-spin effects, *Phys. Rev. D* **98**, 104052 (2018).
- [20] T. Dietrich *et al.*, Matter imprints in waveform models for neutron star binaries: Tidal and self-spin effects, *Phys. Rev. D* **99**, 024029 (2019).
- [21] Katerina Chatziioannou, Antoine Klein, Nicolás Yunes, and Neil Cornish, Constructing gravitational waves from generic spin-precessing compact binary inspirals, *Phys. Rev. D* **95**, 104004 (2017).
- [22] Antoine Klein, EFPE: Efficient fully precessing eccentric gravitational waveforms for binaries with long inspirals, [arXiv:2106.10291](#).
- [23] Katerina Chatziioannou, Antoine Klein, Neil Cornish, and Nicolas Yunes, Analytic Gravitational Waveforms for Generic Precessing Binary Inspirals, *Phys. Rev. Lett.* **118**, 051101 (2017).
- [24] Theodoros A. Apostolatos, Curt Cutler, Gerald J. Sussman, and Kip S. Thorne, Spin induced orbital precession and its modulation of the gravitational wave forms from merging binaries, *Phys. Rev. D* **49**, 6274 (1994).
- [25] Michael Kesden, Davide Gerosa, Richard O’Shaughnessy, Emanuele Berti, and Ulrich Sperhake, Effective Potentials and Morphological Transitions for Binary Black-Hole Spin Precession, *Phys. Rev. Lett.* **114**, 081103 (2015).
- [26] Davide Gerosa, Michael Kesden, Ulrich Sperhake, Emanuele Berti, and Richard O’Shaughnessy, Multi-time-scale analysis of phase transitions in precessing black-hole binaries, *Phys. Rev. D* **92**, 064016 (2015).
- [27] Thibault Damour, Coalescence of two spinning black holes: An effective one-body approach, *Phys. Rev. D* **64**, 124013 (2001).
- [28] Etienne Racine, Analysis of spin precession in binary black hole systems including quadrupole-monopole interaction, *Phys. Rev. D* **78**, 044021 (2008).
- [29] Eric Poisson, Gravitational waves from inspiraling compact binaries: The quadrupole moment term, *Phys. Rev. D* **57**, 5287 (1998).
- [30] Jan Steinhoff, Tanja Hinderer, Tim Dietrich, and Francois Foucart, Spin effects on neutron star fundamental-mode dynamical tides: Phenomenology and comparison to numerical simulations, *Phys. Rev. Res.* **3**, 033129 (2021).
- [31] J. Aasi *et al.*, Advanced LIGO, *Classical Quantum Gravity* **32**, 074001 (2015).
- [32] R. Abbott *et al.* (LIGO Scientific, VIRGO, KAGRA), Tests of General Relativity with GWTC-3, [arXiv:2112.06861](#).
- [33] N. V. Krishnendu, K. G. Arun, and Chandra Kant Mishra, Testing the Binary Black Hole Nature of a Compact Binary Coalescence, *Phys. Rev. Lett.* **119**, 091101 (2017).
- [34] N. V. Krishnendu, M. Saleem, A. Samajdar, K. G. Arun, W. Del Pozzo, and Chandra Kant Mishra, Constraints on the binary black hole nature of GW151226 and GW170608 from the measurement of spin-induced quadrupole moments, *Phys. Rev. D* **100**, 104019 (2019).
- [35] Horng Sheng Chia, Thomas D. P. Edwards, Richard N. George, Aaron Zimmerman, Adam Coogan, Katherine Freese, Cody Messick, and Christian N. Setzer, Dimensionally Reduced Waveforms for Spin-Induced Quadrupole Searches, [arXiv:2211.00039](#).
- [36] Hideyuki Tagoshi, Shuhei Mano, and Eiichi Takasugi, Post-Newtonian expansion of gravitational waves from a particle

- in circular orbits around a rotating black hole: Effects of black hole absorption, *Prog. Theor. Phys.* **98**, 829 (1997).
- [37] Eric Poisson and Misao Sasaki, Gravitational radiation from a particle in circular orbit around a black hole. 5: Black hole absorption and tail corrections, *Phys. Rev. D* **51**, 5753 (1995).
- [38] Kashif Alvi, Energy and angular momentum flow into a black hole in a binary, *Phys. Rev. D* **64**, 104020 (2001).
- [39] F. Acernese *et al.*, Advanced Virgo: A second-generation interferometric gravitational wave detector, *Classical Quantum Gravity* **32**, 024001 (2015).
- [40] B. P. Abbott *et al.*, Prospects for observing and localizing gravitational-wave transients with Advanced LIGO, Advanced Virgo and KAGRA, *Living Rev. Relativity* **21**, 3 (2018).
- [41] Huan Yang, William E. East, Vasileios Paschalidis, Frans Pretorius, and Raissa F.P. Mendes, Evolution of highly eccentric binary neutron stars including tidal effects, *Phys. Rev. D* **98**, 044007 (2018).
- [42] Huan Yang, Inspiralling eccentric binary neutron stars: Orbital motion and tidal resonance, *Phys. Rev. D* **100**, 064023 (2019).